EFFECTS OF ZrO_2 ADDITIONS ON SINTERING OF LiF FLUXED $BaTiO_3$ CERAMICS

by

HYUNG-KOOK YANG

Submitted in Partial Fulfillment of the Requirement

for the Degree of

Master of Science in Engineering

in the

Materials Engineering Program

Richard W. Jones — 17 JUNE 1992

Advisor — Date

Sally M. Hotchkiss — June 19, 1992

Dean of the Graduate School — Date

YOUNGSTOWN STATE UNIVERSITY

JUNE 1992

ABSTRACT

EFFECTS OF ZrO_2 ADDITIONS ON SINTERING OF LiF FLUXED $BaTiO_3$ CERAMICS

HYUNG-KOOK YANG

Master of Science in Engineering

Youngstown State University, 1992

The sintering of barium titanate ($BaTiO_3$) ceramics with 1 and 2 wt% LiF was studied. LiF-fluxed $BaTiO_3$ compacts were sintered to near theoretical density at temperatures below 1100°C in 2 hr. The rapid densification was directly dependent on the LiF content. The crystal structure of LiF flux phase varies during sintering from tetragonal to pseudocubic and then to a second tetragonal symmetry. Microstructure analysis showed a uniform grain size ($\approx$ 1 μm) with 0.75 wt% ZrO_2 added to the flux phase as a grain growth inhibitor. X-ray diffraction studies showed that small-grained samples indicated the suppression of the tetragonal symmetry toward a more cubic modification.

ACKNOWLEDGMENTS

I would like to thank my Heavenly God made this project completed successfully.

I would also like to thank Dr. R. W. Jones, Director, Department of Materials Engineering, for his technical guidance and help throughout the studies.

I would like to express a great appreciation to my parents who have thoroughly supported me all the times.

Special thanks go to my uncle, Mr. Hee S Park, for his help while staying in the States and Mr. Richard Lee Blosser for his techincal advice on SEM studies.

TABLE OF CONTENTS

TABLE OF CONTENTS (cont'd)

LIST OF FIGURES

LIST OF FIGURES (cont'd)

LIST OF FIGURES (cont'd)

LIST OF TABLES

I. INTRODUCTION

Basic ceramic capacitor materials in use today are barium titanate ($BaTiO_3$) and other perovskite materials.[1] In the perovskite lattice, substitution of compatible cations such as Ca, Pb, Zr and Zn provide the necessary control in the selection of suitable dielectric constants, temperature-resistance coefficients, and dielectric losses.[2] These dielectric materials are normally sintered at temperatures between about 1300°C and 1400°C, and often require extended sintering times. Because of the tendency toward miniaturization of electronic components, ceramics with high dielectric constants and low sintering temperatures have become commercially important in order to lower fabrication costs.[3] In multilayer ceramic capacitor fabrication methods they allow the use of base metal electrode systems such as Ni and Cu, replacing the more expensive Ag-Pd noble metal systems now used.[4,5] In order to prevent oxidation of these base metal systems, the capacitor must be sintered in a reducing atmosphere and at lower temperature.[6]

The lower sintering temperatures have typically been achieved by small additions of flux agents to promote liquid phase sintering.[6] Even though liquid state sintering lowers

the sintering temperature, a low dielectric constant intergranular phase, and overall dilution of the dielectric behavior of the $BaTiO_3$ have been observed.[7] However, dilution of the properties can be avoided if reactive liquid phase sintering takes place. In this regard, fluxing agents such as LiF[3,8,9], NaF[9] and B_2O_3[10] have been used to greatly lower the sintering temperature of $BaTiO_3$ and preserve the original dielectric properties. However, very long sintering times were necessary to obtain proper dielectric properties which led to large grains and nonuniform microstructures.[8]

Small additions of ZrO_2 to $BaTiO_3$ have resulted in a reduction of the grain size and a more uniform microstructure. At sintering temperatures below 1350°C, the ZrO_2 resides at the grain boundaries and acts as a grain growth inhibitor. The decrease in grain size was found to increase the permittivity and produce a leveling effect on capacitance versus temperature.[11] Sintering with small additions of ZrO_2 can develop the fine and uniform grain size in the microstructure.

The aim of this study was not only to improve the sintering densification, but also to control the grain growth of LiF fluxed $BaTiO_3$ compacts at temperatures below 1150°C with ZrO_2. The effect of ZrO_2 addition on the crystal structure of fluxed $BaTiO_3$ compacts was also investigated.

II. LITERATURE SURVEY

2.1. Barium Titanate

2.1.1. Crystal Structure

If large dipole moments are developed with each unit cell, there may be a spontaneous interaction between the dipoles of neighboring cells.[12] This interaction, which is called ferroelectric behavior of solids, produces a hysteresis curve. The best-known ferroelectric material is barium titanate ($BaTiO_3$) and is representative of the so-called oxygen octahedron group of ferroelectric materials.[13] Ferroelectric barium titanate is the cubic ABO_3 perovskite structure[2], Figure 1, which occurs between the Curie temperature (≈120°C) and 1460°C.

The perovskite structure is characterized by a network of corner-linked oxygen octahedra with the smaller cations filling the octahedral sites and the larger cations filling the dodecahedral interstices.[2] Above the Curie temperature, the Ba^{2+} and O^{2-} ions combine to form a close-packed cubic structure with the smaller, more highly charged Ti^{4+} ions in octahedral interstices. Each O^{2-} is surrounded by four Ba^{2+} and eight O^{2-}, each Ba^{2+} is surrounded by twelve O^{2-}. In the center of the face centered cubic unit cell Ti^{4+} is octahedrally coordinated to six O^{2-}. When the temperature is

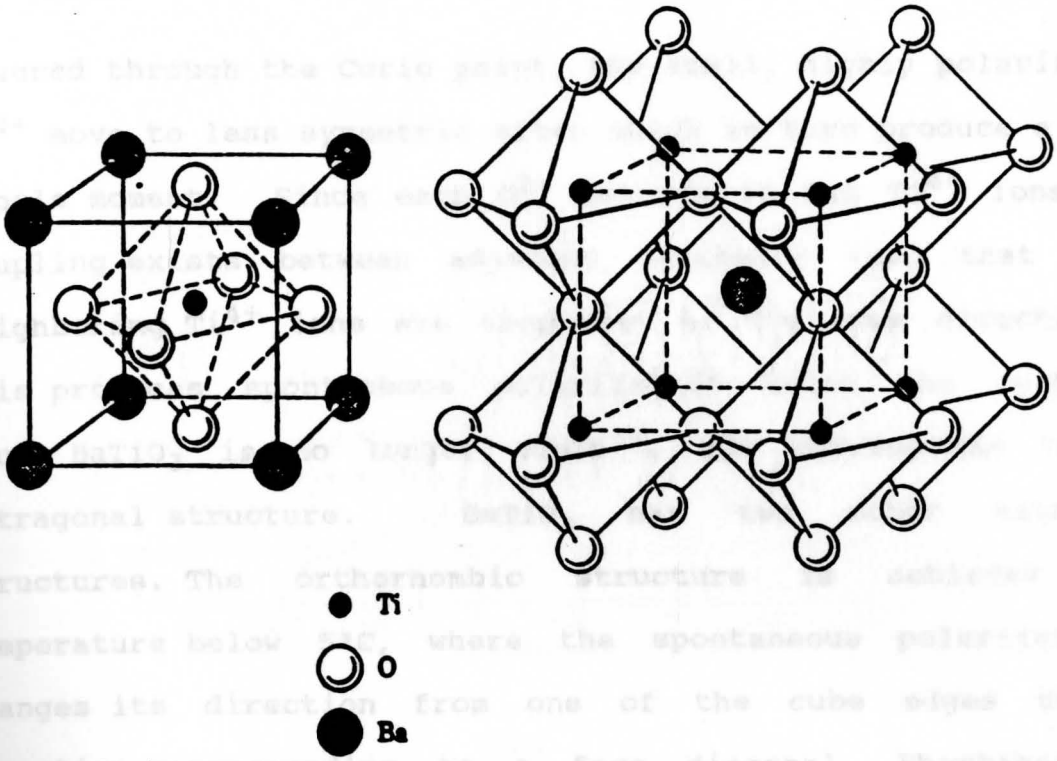

Figure 1. Ion positions in ideal cubic perovskite structure.

Table 1.

Phase transformations of $BaTiO_3$

Phase	Temperature (°C)
Hexagonal	> 1460
Cubic	> 120
Tetragonal	> 5
Orthorhombic	> -90
Rhombahedral	< -90

lowered through the Curie point, the small, highly polarized Ti^{4+} move to less symmetric sites which in turn produce a net dipole moment. Since each O^{2-} belongs to two Ti^{4+} ions, a coupling exists between adjacent octahedra such that the neighboring Ti^{4+} ions are displaced in the same direction. This produces spontaneous polarization along the c-axis. Thus, $BaTiO_3$ is no longer cubic[13], but corresponds to a tetragonal structure. $BaTiO_3$ has two other crystal structures. The orthorhombic structure is achieved at temperature below 5°C, where the spontaneous polarization changes its direction from one of the cube edges to a direction corresponding to a face diagonal. Rhombahedral structure is achieved at -80°C, where the spontaneous polarization changes from a direction corresponding to a face diagonal to one along a body diagonal. The temperature ranges for these phase changes is given in Table 1.

Associated with each of these ferroelectric transitions is a change in the crystal structure of $BaTiO_3$.[13] These transition temperatures, reflected in the dielectric constants and in the lattice parameters, are shown in Figure 2. When selecting the adequate operating temperature to utilize $BaTiO_3$, it is very important to understand where the phase transformations take place and their effect on the resulting properties.

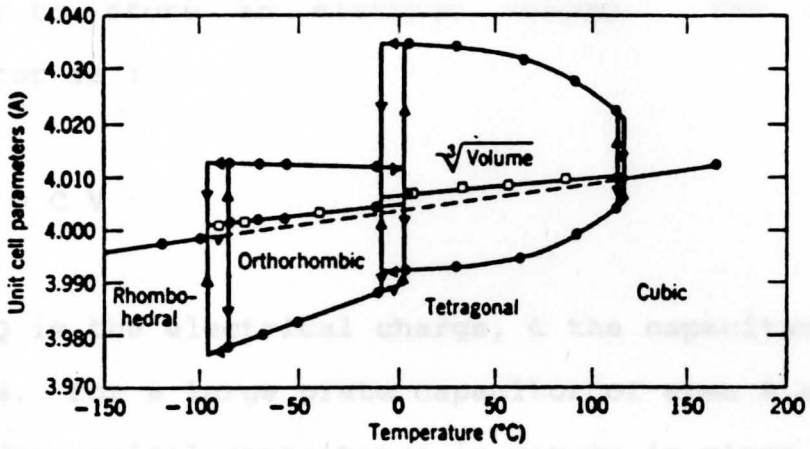

(a)

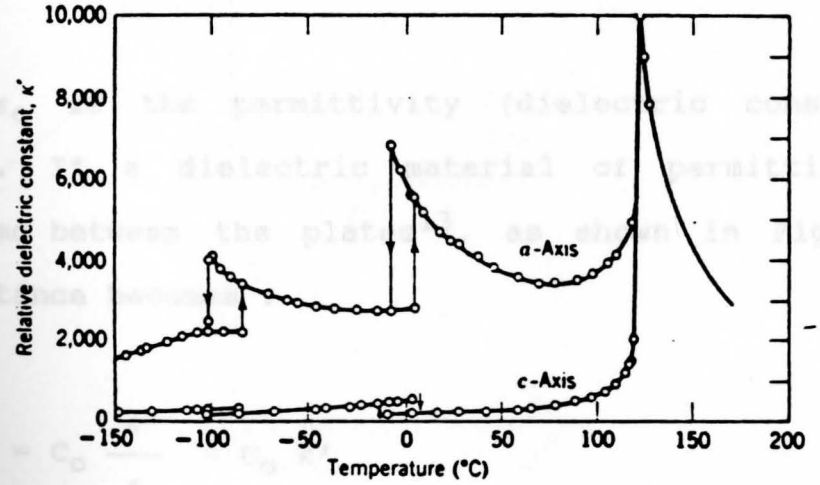

(b)

Figure 2. (a) Lattice parameters of $BaTiO_3$ as a function of temperature. (b) Dielectric constant of $BaTiO_3$ as a function of temperature.[2]

2.1.2. Properties

(A). Relative Permittivity

The principle characteristic of a capacitor is its ability to store an electric charge. The charge on a capacitor is :

$$Q = C\ V \tag{1}$$

where Q is the electrical charge, C the capacitance and V the voltage. For a large plate capacitor of area A and thickness *d* the geometrical capacitance in vacuum is given by :

$$C_o = (\ A/d\ )\ \epsilon_o \tag{2}$$

where ϵ_o is the permittivity (dielectric constant) of a vacuum. If a dielectric material of permittivity ϵ' is inserted between the plates[13], as shown in Figure 3, the capacitance becomes :

$$C = C_o \frac{\epsilon'}{\epsilon_o} = C_o\ k' \tag{3}$$

where k' is the relative permittivity or relative dielectric constant. It is defined as the ratio of the permittivity of

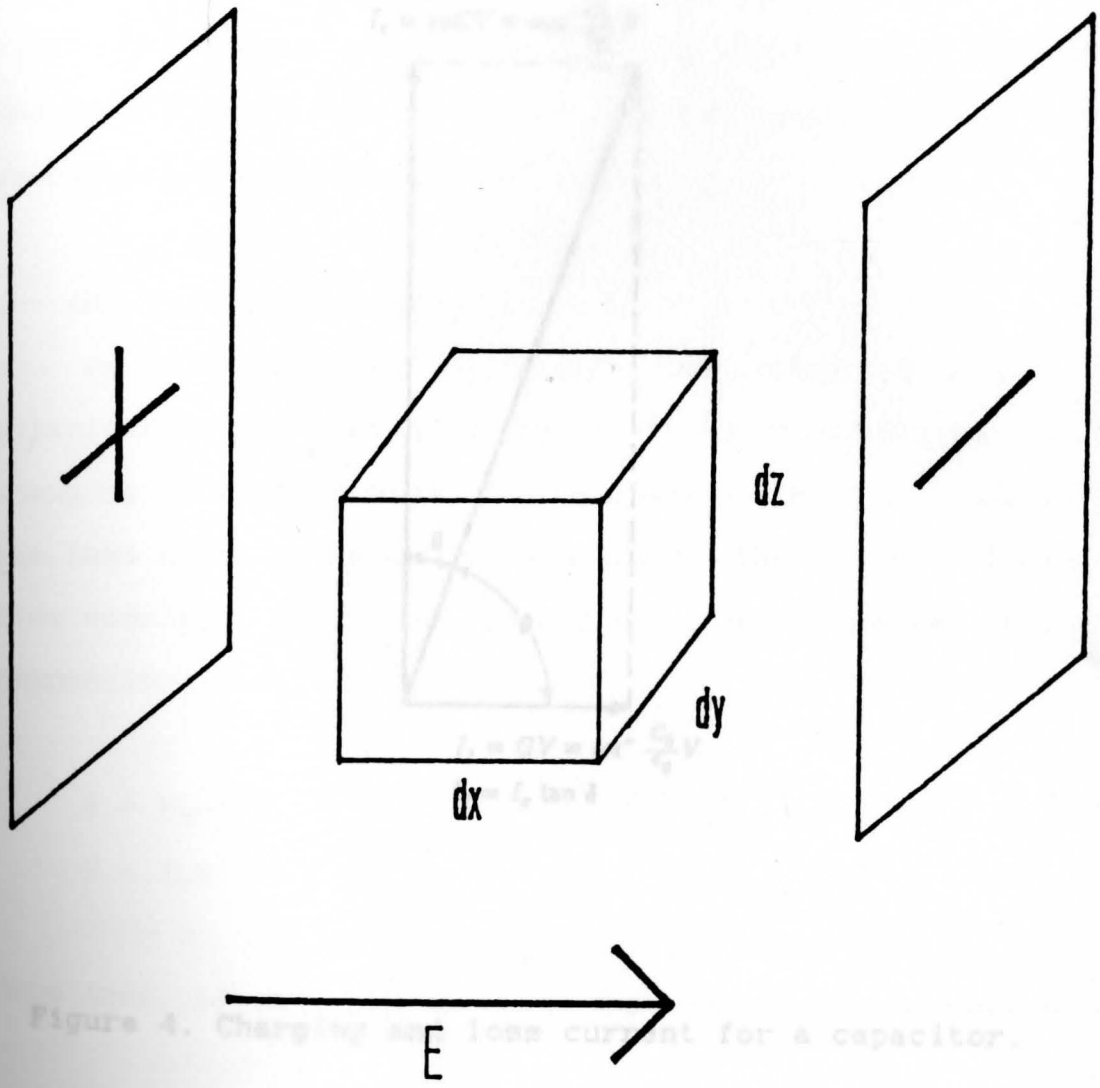

Figure 3. Illustrating a cavity dx dy dz away from a dielectric between two charged plates.

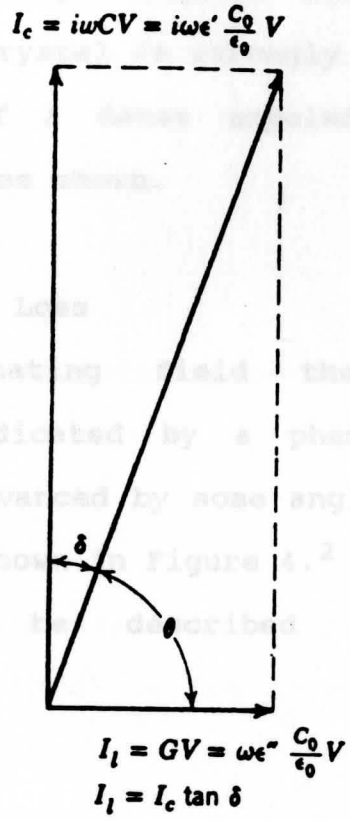

Figure 4. Charging and loss current for a capacitor.

a medium, ϵ', to the permittivity of free space, ϵ_o.

The relative permittivity of $BaTiO_3$ is affected by temperature, density, frequency, and grain size.[14] The effect of temperature on single crystal $BaTiO_3$ is shown[2], [Figure 2(b)]. The single crystal is strongly anisotropic, therefore, the permittivity of a dense unpoled sample should be an average of the values shown.

(B). Dielectric Loss

For an alternating field the time required for polarization is indicated by a phase retardation of the changing current advanced by some angle $(90 - \delta)$, where δ is the loss angle as shown in Figure 4.[2] The electric field and flux density can be described by complex notation respectively as :

$$E = E_o e^{iwt} \tag{4}$$

$$D = D_o e^{i(wt-\delta)} \tag{5}$$

From Eqns. (4) and (5) the flux density can be defined as :

$$D = K^* E \tag{6}$$

where K^* is the complex dielectric constant. Mathematical

manipulation of Eqns. (5) and (6) leads to an expression of the complex dielectric constant as :

$$K^* = K_s e^{-i\delta} = K_s(\cos\delta - i\sin\delta) \quad (7)$$

where $K_s = D_o/E_o$ and is represented as the static dielectric constant. Separation of complex variables gives :

$$K' = K_s\cos\delta \quad (8)$$

$$K'' = K_s\sin\delta \quad (9)$$

from which the loss tangent can be defined as :

$$\tan\delta = K''/K' = E''/E' \quad (10)$$

Often associated with the loss tangent is the Q factor, a figure of merit, defined as the inverse of the loss tangent ($Q = 1/\tan\delta$).

(C). Piezoelectricity

When an applied field induces dipole moments in atoms or ions, the dimensions of a specimen undergo slight changes. In most materials dielectric polarization produces a mechanical distortion, but mechanical distortion does not produce polarization.[13] This electromechanical effect, which is present in all materials, is called electrostriction.

In pure electrostrictive materials, the mechanical deformation produced by a polarization in a given direction is the same as that produced by a polarization in the opposite direction.[13] Figure 5 shows a simple example of a material with only electrostrictive properties. Application of a field along the positive *x*-direction produces the same mechanical deformation as a field along the negative *x*-direction. The dashed square is the basic unit and has a center of symmetry.

There are solid dielectric materials, however, for which the sign of a mechanical deformation produced by a polarization changes when the direction of the polarization is reversed. These materials are polarized upon application of a mechanical stress and are called "piezoelectric." They are of practical importance because they permit conversion of mechanical into electrical energy and vice versa. A two-dimensional example of such a material is represented in Figure 6. The basic unit from which this material can be built lacks a center of symmetry, and this is a requirement for a piezoelectric material.[13] If a tension along the *x*-direction is applied in Fig. 6, the angle θ will increase, thus giving rise to a polarization in the positive *y*-direction.

But if the unit is compressed along the x-direction, θ will decrease and the polarization will lie along the negative *y*-direction.[13] However, application of tension or compression to the basic unit in Fig. 5 produces no polarization at all, because of the symmetry of the unit.

2.1.3. Stoichiometry

The sintering behavior, microstructure and dielectric properties of pure $BaTiO_3$ are greatly affected by the relative cation concentrations or stoichiometry.[15] Figure 7 compares stoichiometric $BaTiO_3$ (a) to samples containing 1 mol% TiO_2 (b), and 2 mol% excess BaO (c).[14] It is found that TiO_2 enhanced grain growth while BaO acted as a grain refiner or grain growth inhibitor. Titania enhanced grain growth can be explained by examining the Ti rich region of $BaO{\cdot}TiO_2$ phase diagram, Figure 8. This region indicated the formation of a liquid phase above 1322°C, which results in enhanced diffusion during sintering.

Negas *et al.*[16] identified the crystalline compound in the Ti rich region as $Ba_6Ti_{17}O_{40}$. Smaller excesses of either BaO or TiO_2 also influence the microstructure, density and dielectric behavior of $BaTiO_3$. However, large increases in the cationic ratio result in increased enclosed porosity,

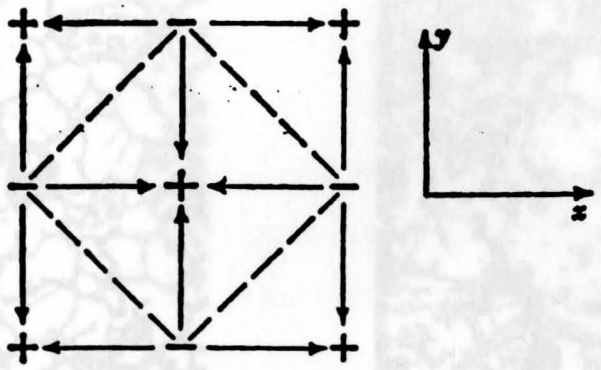

Figure 5. A two-dimensional square lattice with only electro-strictive properties.

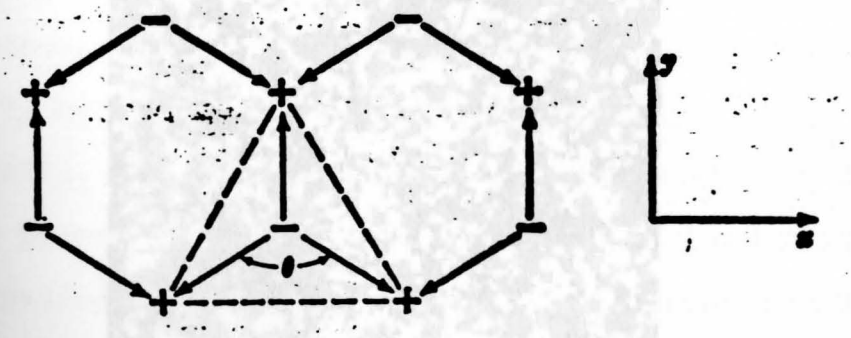

Figure 6. A two-dimensional structure with piezoelectric properties.

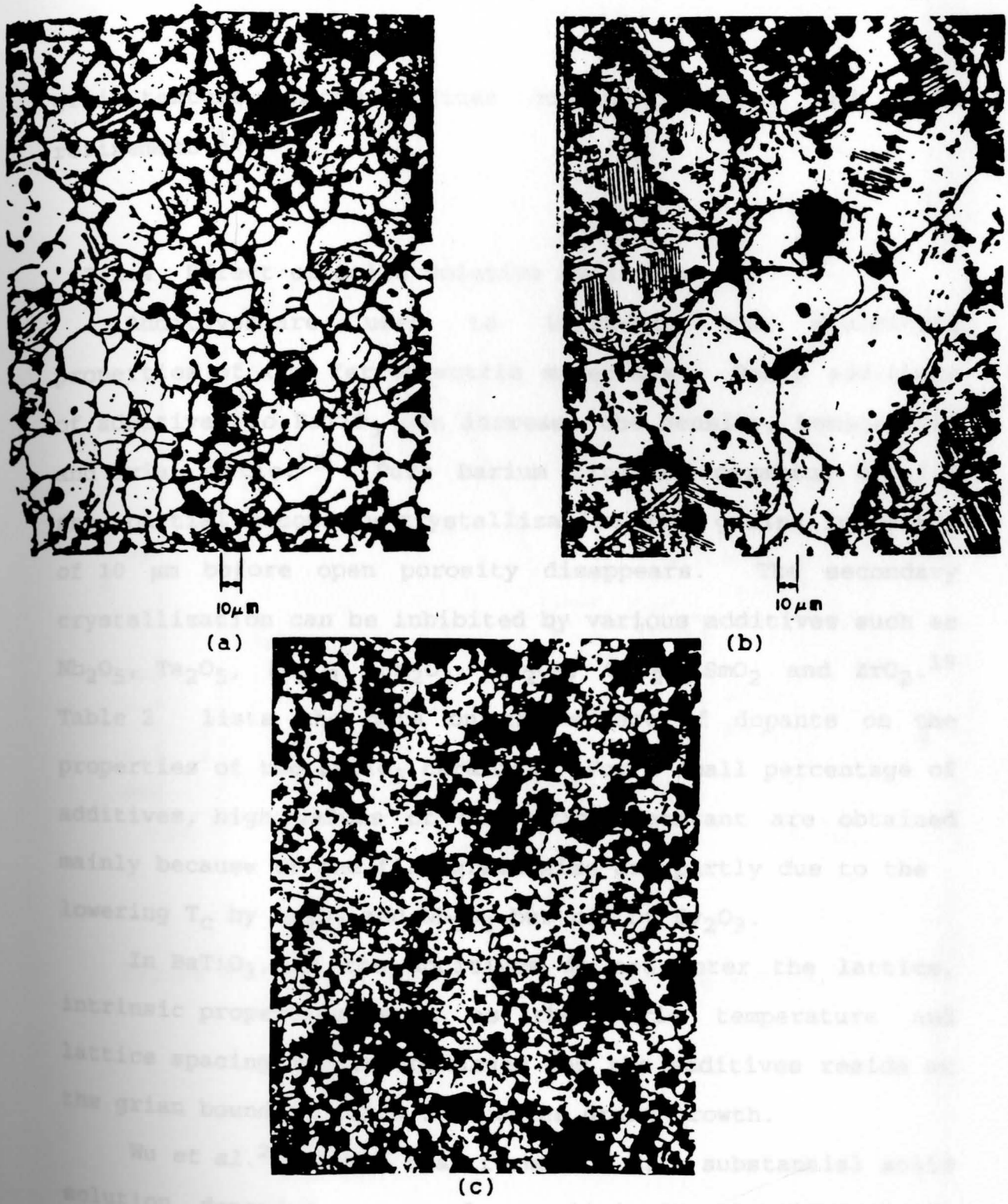

Figure 7. $BaTiO_3$ fired in air (a) Stoichiometric (b) 1 mol% excess TiO_2 (c) 2 mol% excess BaO.[15]

grain texture changes, finer domain patterns, and grain refinement.[16]

2.1.4. Effect of Solid Solution Additives

Additives are used to influence the dielectric properties of the ferroelectric materials. Small additions of additives to $BaTiO_3$ can increase the density, homogeneity and axial ratio.[18] Pure barium titanate ceramics usually show partial secondary crystallization with grains in excess of 10 μm before open porosity disappears. The secondary crystallization can be inhibited by various additives such as Nb_2O_5, Ta_2O_5, La_2O_3, Sm_2O_3, Dy_2O_3, TiO_2, SmO_2 and ZrO_2.[19] Table 2 lists the data on the effect of dopants on the properties of the $BaTiO_3$ ceramics. For a small percentage of additives, high values of dielectric constant are obtained mainly because of the fine grain size and partly due to the lowering T_c by La_2O_3 and Nb_2O_3 but not by Dy_2O_3.

In $BaTiO_3$, if the additives do not enter the lattice, intrinsic properties such as the Curie temperature and lattice spacing remain unchanged and the additives reside at the grian boundary which influences grain growth.

Wu *et al.*[20] showed that formation of a substantial solid solution depended on at least limited solubility of the

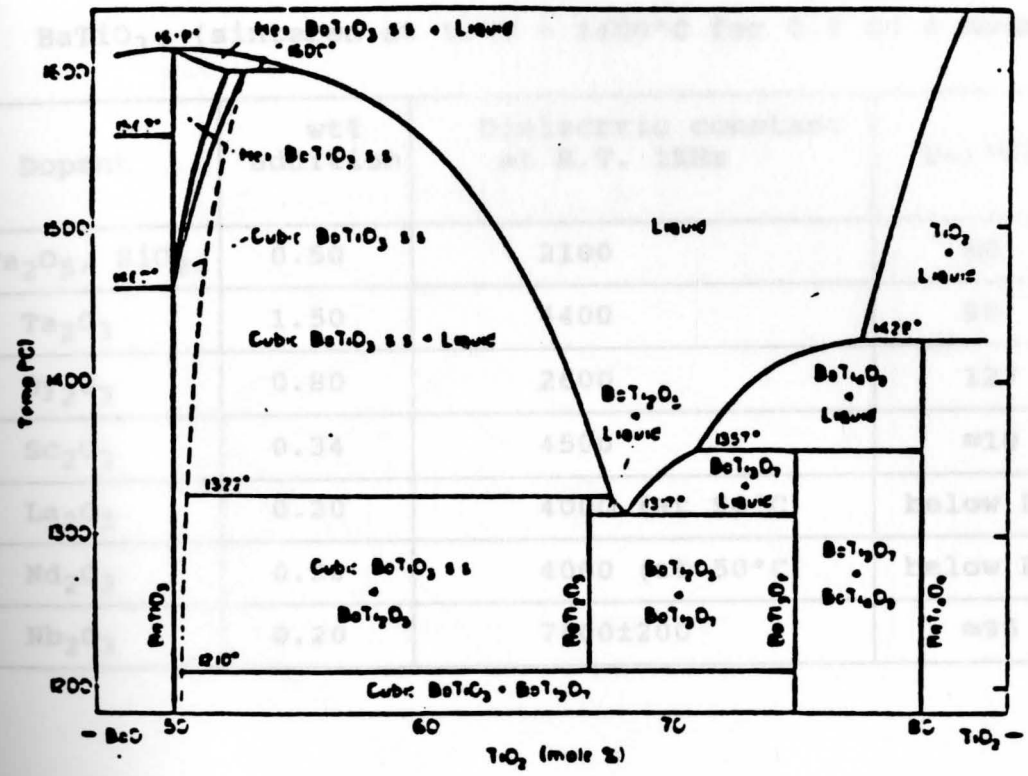

Figure 8. Phase diagram for the BaO-TiO_2 system.[15]

Table 2. Effects of different dopants on the properties of $BaTiO_3$. (sintered at 1200 - 1400°C for 0.5 to 4 hours)

Dopant	wt% addition	Dielectric constant at R.T. 1KHz	Tc(°C)
Ta_2O_5, SiO_2	0.50	2100	40
Ta_2O_3	1.50	4400	90
Dy_2O_3	0.80	2600	123
Sc_2O_3	0.34	4500	≈10
La_2O_3	0.20	4000 (at 50°C)	below R.T.
Nd_2O_3	0.20	4000 (at 50°C)	below R.T.
Nb_2O_3	0.20	7800±200	≈95

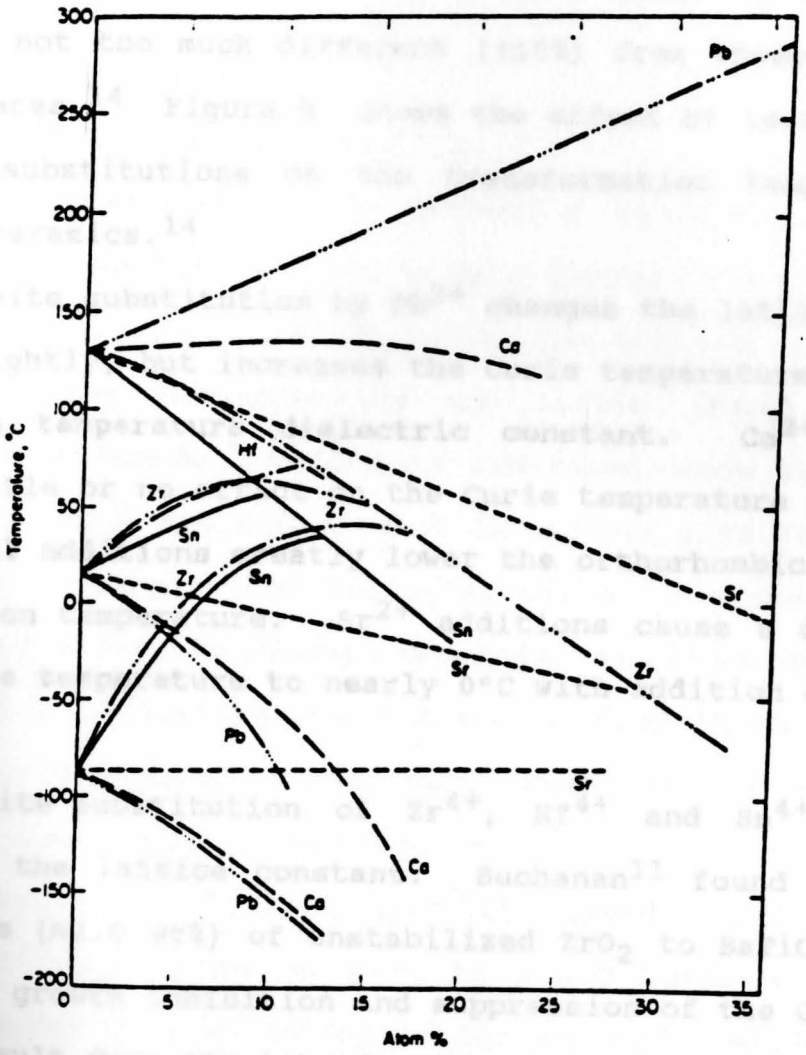

Figure 9. Effect of isovalent substitutions on the transition temperature of $BaTiO_3$.[14]

additives on either the A or B site of $BaTiO_3$. The condition for this occurrence is when the ionic radii of the additive ion are not too much different (±15%) from those of the ion it replaces.[14] Figure 9 shows the effect of isovalent A and B site substitutions on the transformation temperature of $BaTiO_3$ ceramics.[14]

A-site substitution by Pb^{2+} changes the lattice constant only slightly, but increases the Curie temperature and lowers the room temperature dielectric constant. Ca^{2+} additions have little or no effect on the Curie temperature at ≈ 120°C, but small additions greatly lower the orthorhombic-tetragonal transition temperature. Sr^{2+} additions cause a decrease in the Curie temperature to nearly 0°C with addition of ≈30 atom percent.

B-site substitution of Zr^{4+}, Hf^{4+} and Sn^{4+} for Ti^{4+} increase the lattice constant. Buchanan[11] found that small additions (≈2.0 wt%) of unstabilized ZrO_2 to $BaTiO_3$ resulted in grain growth inhibition and suppression of the Curie peak. These result from the introduction of the larger ions such as Zr^{4+} into the octahedral sites, resulting in a reduced Curie temperature dielectric constant.

Substitution by similar size ions such as Y^{3+} and Bi^{3+} increase the Curie temperature[14] and are the only ions which do so besides Pb^{2+} and Cu^{2+}. Of these additives which lower

the Curie temperature some shift the dielectric peak, while others broaden the peak. Additives which cause broadening to occur are Nb^{5+}, Ta^{5+}, In^{5+} and La^{5+}.[14]

2.1.5. Effect of Flux Additives

In general, the lower sintering temperature has been achieved by adding to the ceramic powder small amounts of flux agents, or a quantity of a low melting glass powder which promotes densification by liquid phase sintering. There are a number of fluxing additions such as LiF,[3,8,9] B_2O_3,[7,10] CuO_2[1] and V_2O_5[21] that have been used to lower the sintering temperature of $BaTiO_3$ ceramics. The use of LiF has successfully led to dense compacts at temperature below 1000°C with preserving the dielectric properties. However, very long sintering times were required to obtain the original dielectric properties.

Walker *et al.*[9] found that LiF aided densification of $BaTiO_3$ at temperature as much as 500°C lower than without additives for both sintering in air and hot pressing. It was also observed that a combination of 1 wt% LiF and 2 wt% MgO resulted in an increase of almost 100% in strength of $BaTiO_3$. This increase caused much lower internal stresses. The effects of several other halides on hot pressing of $BaTiO_3$ were also studied. It was found that rapid densification

began at 650°C when FLiNaK (mp = 450°C) or NH_4F was added, 800°C -900°C with BaF_2 and 1000°C - 1100°C with additions of most other halides such as LiCl, MgF_2 and NaF.

Anderson *et al.*[22] concluded that sintering of $SrTiO_3$ with LiF to near theoretical densities was dependent on the cationic ratio, the LiF content, and the temperature. It was observed that Li substituted for Ti in the $SrTiO_3$ crystal structure. Grain boundary analysis showed proof of a Ti rich amorphous phase.

Haussonne *et al.*[8] studied the effect of LiF and the cationic ratio on the microstructure and dielectric properties of $BaTiO_3$. It was found that the Li and F content decreased with temperature leaving a single phase structure.

Castelliz *et al.*[10] found that B_2O_3 was an effective flux agent at up to 20 mol% addition. It was found to lower the sintering temperature and improve the mechanical properties of mixed ceramic bodies. The dielectric constant decreased as the flux additions increased above 10 mol%, while dielectric loss and insulation resistance decreased with increasing flux content.

2.2. Preparation of Barium Titanate Powders

The dielectric properties' dependence on particle size can be reduced if powders can be prepared with an average crystallite size of ≤1000 Å. The three important methods for preparation of $BaTiO_3$ powders are reviewed here.

2.2.1. Thermochemical Method

This is based on the solid state reaction between $BaCO_3$ and TiO_2. With an equimolar mixture of $BaCO_3$ and TiO_2, Ba_2TiO_4, $BaTi_3O_7$ and the hexagonal $BaTiO_3$ are as likely to form as $BaTiO_3$ depending on temperature,[23,24] incomplete mixing or reduction, disequilibrium, and impurities. Formation of Ba_2TiO_4 is particularly harmful since it is hygroscopic and decomposes with swelling which results in cracking or crazing of the ceramic, in addition to having poor loss characteristics.[14] A temperature for the formation of $BaTiO_3$ powder is generally 1350°C.[24] The reaction rate between $BaCO_3$ and TiO_2 was found to decrease with increasing partial pressure of CO_2 or N_2, but to increase with increase in the oxygen partial pressure. This behavior was attributed to equilibrium defects in the oxide and interfacial reactions between the participating species.

2.2.2. Pyrolytic Decomposition

Fine powders of high purity $BaTiO_3$ are synthesized by the pyrolytic decomposition of certain coprecipitated products such as oxalates,[25] citrates[26] and carbonate-hydrooxide mixtures. The decomposition temperature is extremely important since it determines the particle size and sinterability of the powders. For example, the decomposition of barium titanyl oxalate tetrahydrate $BaTiO(C_2H_4)_2 \cdot 4H_2O$ at temperature varying from 550° to 1150°C results in particle size variation of 400 to 3000 Å.

The product of low temperature decomposition was found to give agglomerated porous particles of low density and high surface energy causing low green and fired ceramic densities. The product of high temperature decomposition, on the other hand, was found to be less active and higher density particles with a wide distribution of particle sizes. These characteristics lead to exaggerated grain growth and to lower fired densities. The optimum temperature of decomposition was recommended to be around 900°C.

For the coprecipitation of citrates of barium and titanium, Mulder has used a method in which the aqueous solutions of atomized citrates are sprayed as droplets in an alcohol medium.[26] The coprecipitation takes place by the dehydration of individual droplets by alcohol. Since each

drop gives rise to one powder particle, it is possible to maintain stoichiometry. The optimum decomposition temperature was 700 - 800°C. The resulting powders are dense, coagulated globular or rod shaped particles of 3 - 10 μm size, which results in a ceramic density of 99%.

2.2.3. Metal Alkoxide Decomposition

In this method a simultaneous hydrolytic decomposition of a mixture of the respective metal alkoxides yields a stoichiometric, high purity and ultrafine powders (55 -150Å). Mixing of very small concentrations of dopant material is possible at nearly the molecular level. Thus, using appropriate metal alkoxide mixtures, barium titanate powders with various dopants such as Sc_2O_3, La_2O_3, Nd_2O_3 and Nb_2O_5 with dopant concentrations varying of 0.1 to 0.34 mol% were prepared. Calcining these powders at temperature greater than 500°C is found to significantly change their reactivities. From these powders, highly dense, fine grained bodies of uniform microstructures having better physical properties are achieved than are obtained by using conventional cold pressing and sintering methods (Table 3 & 4).

2.2.4. Comparison of The Three Methods

Among the three methods, the thermochemical method is the least expensive and is most commonly used in the industry despite the lower purity and not-so-fine particle size of the powders. The coprecipitation, although it yields higher purity powder, is more expensive and does not give as good piezoelectric properties as does the thermochemical method. Moreover, higher purity makes sintering more difficult. The alkoxy synthesis is the most sophisticated and expensive process, and yields stoichiometric powders of high purity and fine particle size which are likely to have potential applications in special microwave and electrooptic devices.[27] Powder stoichiometry can be better maintained by this method than by the other two methods.

2.3. Densification

2.3.1. Solid State Sintering

Sintering process is composed of three basic steps: binder removal, densification, and grain growth.[22] Solid state sintering involves material transport by diffusion. Diffusion is characterized by movements of atoms or vacancies along surfaces, grain boundaries or through the volume of the material.[28] Surface diffusion, like vapor - phase

Table 3. Characteristic of $BaTiO_3$ powders prepared by different methods

Characteristic	Powders		
	Alkoxide	Chemically pure	Commercial
Surface area (m^2/gm)	57	3.5	1.3
Crystal size (μm)	0.025	0.3	1.5
Agglomerate size (μm)	0.25	1	1
Ratio $BaO:TiO_2$	1.000	1.000	1.01

Table 4. Properties of $BaTiO_3$ powders prepared by different methods

Method and sintering schedule	% Theoretical density	Average grain size (μm)	Dielectric constant
Thermochemical 1400°C	>96	1 - 5	1500
Oxalate derived			
1300°C -- 2 hr	84	> 1	2100
1350°C -- 2 hr	95	2	2600
1400°C -- 2 hr	95	300	1500
Citrate based			
1300°C -- 2 hr	91	3	1400
1350°C -- 2 hr	97	0.3	1300

transport, does not result in shrinkage. The driving force for solid-state sintering is the difference in free energy or chemical potential between the free surfaces of particles and the points of contact between adjacent particles.

Kingery *et al.*[29] derived the following equation for the mechanism of transport of material by lattice diffusion from the line contact between two particles to the neck region :

$$\frac{\delta L}{L_o} = \left[\frac{20\ \tau\ a^3\ D^{2/5}}{\sqrt{2}\ k\ T} \right] r^{-6/5}\ t^{2/5} \qquad (11)$$

where: $\delta L/L_o$ = Fractional Shrinkage

D = Self diffusion Coefficient

r = Particle Radius

k = Boltzmann's Constant

T = Absolute Temperature

a^3 = Vacancy Volume

τ = Surface Free Energy

t = Time

Equations for other volume diffusion mechanisms of sintering are quite similar.[29] In each case the rate of shrinkage increases with increasing temperature and with decreasing

particle radius and decreases with time. Control of temperature and particle size is extremely important in sintering process, but control of time is less important.

When grain growth begins, the average distance between pores increases. As grains grow the pores are dragged by the moving grain boundary. The numerous small moving pores tend to coalesce into fewer large pores. Thus, the average pore size increases through coalescence, even though the total volume of pores may be decreasing. This pore growth further reduces the driving force for sintering.[28]

In the final stage of sintering, when closed pores are present, grain growth can trap the pores within the grains. The energetically favored structure is that in which the closed porosity occupies four-grain corners.[30] An alternate final stage takes place when discontinuous grain growth occurs before all porosity is removed.

2.3.2. Liquid Phase Sintering

A number of ceramic materials can be prepared from powders by liquid-phase sintering. In this process, conditions of temperature and powder composition are chosen so that a quantity of liquid, usually small (a few volume percent or less), is formed between the remaining grains of

the powder. Microstructure changes result from three steps in liquid-phase sintering: (i) rearrangement, (ii) solution-precipitaion, and (iii) coalescence.[29] During sintering, the liquid fills the pores and capillaries and draws the particles together, causing the voids to disappear and the volume to decrease. The presence of the liquid phase markedly increases the densification rate over that of solid-state sintering and near-theoretical densities are routinely achieved in a short sintering time.[29] The rate controlling factors in liquid phase sintering are viscosity, surface tension of the liquid-vapor interface, and the initial particle size of the powder.

Assuming a system where the particles are spherical and perfect wetting occurs, the surface energy relationships for wetting of the solid and complete penetration of the liquid between the grains require that:[29]

$$\tau_{SV} > \tau_{LV} > \tau_{SS} > 2\tau_{SL} \qquad (12)$$

where τ_{SV}, τ_{LV}, τ_{SS}, and τ_{SL} are the surface energies associated with the solid-vapor, liquid-vapor, solid-solid, and solid-liquid phases respectively. Upon melting, the liquid completely coats the solid particles, eliminating τ_{SV}. Pores are formed in the liquid phase which cause a decrease

in the liquid-vapor pore surface area. It is this decrease in area that is the driving force for liquid phase densification.

A negative pressure is acting on each pore, given by the relation,[29]

$$P^{o} = \frac{-2\tau_{LV}}{r_p} \tag{13}$$

where r_p is the pore radius. This pressure is equivalent to the consolidating pressure on the compact by placing the entire system under a hydrostatic pressure. This pressure initially tends to rearrange particles to give maximum packing. In a two-sphere model the spheres are held together by the capillary pressure given as:

$$P = -\tau_{LV}/r \tag{14}$$

where r is the radius of curvature of the liquid miniscus. The capillary pressure is balanced by substantial compressive forces at the contact points. This capillary pressure results in an increase in the chemical potential and activity of the solid phase at the contact areas according to the relations,[29]

$$\mu - \mu_o = RT \ln \frac{a}{a_o} = \delta P V_o \,, \tag{15}$$

$$\ln \frac{a}{a_o} = \frac{K2\tau_{LV}V_o}{r_p RT} \qquad (16)$$

where V_o = Molecular volume

K = Contact relating the maximum contact area pressure to the overall hydrostatic pressure.

μ, a = Chemical potential and activity of the solid phase in the liquid within the contact area.

μ_o, a_o = Chemical potential and activity of the solid phase in the liquid near the free surface.

The major change in free energy that occurs during densification is due to the decrease in surface area of pores in the liquid phase, and provides the driving force for sintering.

The rearrangement process,[29] the initial stage of liquid phase sintering, involves the formation of a liquid phase leading to particle movement giving maximum packing and minimum porosity. This is taking place due to particles' sliding over one another. The initial step corresponds to a viscous flow process and is followed by resistance to further rearrangement corresponding to plastic flow with some effective yield point. Rearrangement occurs rapidly and is the principal mechanism for shrinkage during liquid phase sintering.

Solution precipitation leads to densification by material transport from the contact point to free surfaces of the solid phase.[29] The solubility of the solid phase at the contact areas is larger than that of other solid surfaces and results in material transport away from the contact area to free surfaces. Accompanying this transport process is a decrease in the center-to-center distance of the particles. In the third stage of the liquid phase sintering, coalescence of grains takes place.[29] Along a line between grain centers material is solid and in order for densification to occur, material must be transferred within the solid phase. Consequently, rapid densification corresponding to liquid phase processes is stopped, and the densification rate decreases.[29]

2.4. Manufacture of Ceramic Capacitors

2.4.1. Principle of Capacitor

The first capacitor, called Leyden jar, was invented by the English astronomer and physician John Bevis in 1746.[31] A Leyden jar is a glass jar lined with metal foil and covered on the outside with a second piece of metal foil. A metal rod pushed through a rubber stopper in the neck of the jar makes contact with the inner foil. Both foils act as electrodes,

but they have no net charge other than what is supplied by an external source. If the source of charge is touched to the metal rod in the Leyden jar, electrons move freely from the source into the jar. A net negative charge is transferred to the inner electrode. Because the storage capacity of the jar is limited by the mutual repulsion of electrons, electrons eventually stop flowing. Similar principles apply to the storage of a net positive charge, generated by the removal of electrons from the inner electrode. The ability to store charge is known as capacitance.

There are two obvious ways to increase the capacitance of a Leyden jar.[32] One way is to increase the surface area of the electrodes, giving the charge more room to spread out and reducing the repulsion force between electrons. The other way is to reduce the thickness of the glass separating the stored inner charge from the neutralizing outer charge. If the glass becomes too thin, however, electrons can be pulled through it, creating a spark that dissipates the charge.[31]

The charge generated on the glass or insulator helps to neutralize the charges on the electrodes, and some insulators can bear charges that are nearly as large as those on the electrodes themselves. Neutralization reduces repulsive forces and allows more charge to reside on the electrodes, increasing capacitance. The degree to which this phenomenon

occurs is reflected in a property of the insulator called the dielectric constant.[12] The glass used in a Leyden jar has a dielectric constant of about 5. New insulators in capacitors now used have dielectric constants of close to 20,000.[31]

2.4.2. Processing

The multilayer ceramic capacitor (MLCC) is a compact version of Leyden jar. In actual manufacturing practice,[31] Figure 10, ceramics consisting of barium titanate and small amounts of other oxides are generally used as the insulator. Fine powders having particles a few micrometers are dispersed in a solvent in which organic binders that will hold the particles together have been dissolved.[31] The resulting slurry has the consistency of paint. This slurry is cast in thin sheets onto a paper or stainless steel belt. Sheet thickness is controlled by a blade that resides a few thousandths of an inch above the belt. The slurry dries as the solvent evaporates, leaving a cohesive "green"(unfired) tape that is smooth and limp like fine cloth. The tape is cut into sheets from six to eight inches. Squares, and thousands of electrodes are printed on each sheet through a thin screen that delineates the electrode patterns. The electrodes are made of Ag-Pd ink, a mixture of finely divided metal particles in an organic binder.

After the electrodes have been printed, 30 to 60 sheets are pressed between several layers of unprinted sheets to form a stack, which is then diced into thousands of individual capacitors. The electrode patterns are offset in opposite directions on successive sheets so that when the sheets are stacked and diced, electrodes on alternating sheets are exposed at both ends of the stack. The green capacitors are fired in a furnace by slow heating to temperature between 1,100 and 1,400°C. The metal particles in the electrodes also sinter during firing, forming continuous metal sheets.

Terminations are applied by dipping the ends of each capacitor in another Ag-Pd ink. The ink is fused by a second firing. Terminations are then plated with Ni to prevent the silver from leaching out, and wire leads can be attached to the terminations for subsequent soldering into a circuit. Frequently the finished MLCC is embedded in plastic to seal out moisture.[32]

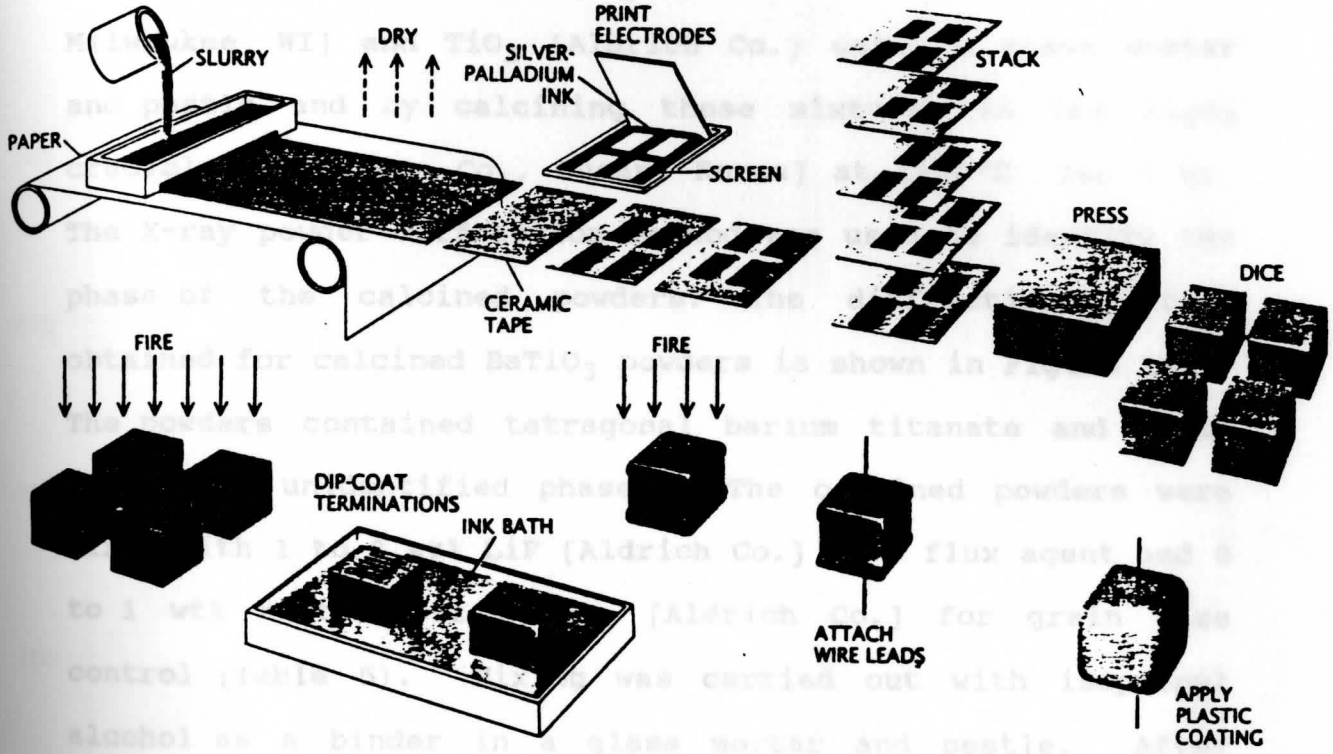

Figure 10. Manufacturing process of MLCC.[31]

III. EXPERIMENTAL PROCEDURE

3.1. Sample Preparation

The $BaTiO_3$ powders with a Ba/Ti atomic ratio of 1.0 were prepared by dry-mixing $BaCO_3$ [Aldrich Chemical Co. Inc., Milwaukee, WI] and TiO_2 [Aldrich Co.] using a glass mortar and pestle and by calcining these mixtures in the Al_2O_3 crucible [Chang Won Co., Pusan, Korea] at 1150°C for 1 hr. The X-ray powder diffraction method was used to identify the phase of the calcined powders. The diffraction pattern obtained for calcined $BaTiO_3$ powders is shown in Figure 11. The powders contained tetragonal barium titanate and small amounts of unidentified phases. The calcined powders were mixed with 1 to 2 wt% LiF [Aldrich Co.] as a flux agent and 0 to 1 wt% unstablilized ZrO_2 [Aldrich Co.] for grain size control (Table 5). Mixing was carried out with isopropyl alcohol as a binder in a glass mortar and pestle. After mixing, the slurries were air dried and dry powders were cold pressed at 136 MPa (20,000 psi). All pellets (0.5 in. diameter) were fired in air on ZrO_2 setter [Chang Won Co.]. The pellets were heated at 10°C/min to sintering temperature and soaked for 0 to 2 hrs, Figure 12. Fired samples were then air quenched. The optimum sintering temperatures and times were based on fired density and microstructure.

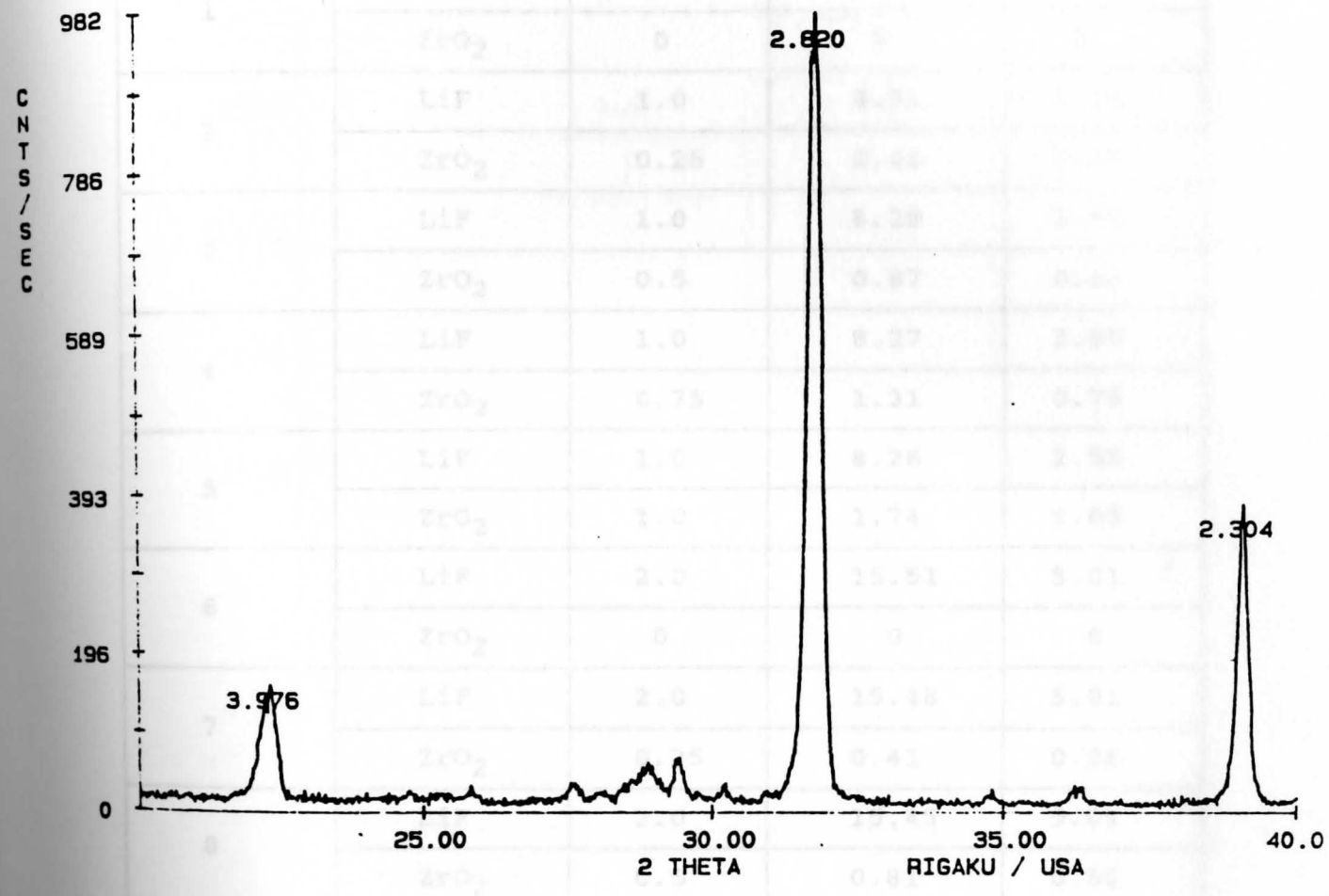

Figure 11. X-ray diffraction pattern of pure $BaTiO_3$ at 25°C.

Table 5. Percent Flux Additions in $BaTiO_3$

Sample #	Additives	Composition (%)		
		wt %	mol %	vol %
1	LiF	1.0	8.33	2.55
	ZrO_2	0	0	0
2	LiF	1.0	8.31	2.55
	ZrO_2	0.25	0.44	0.26
3	LiF	1.0	8.29	2.55
	ZrO_2	0.5	0.87	0.53
4	LiF	1.0	8.27	2.55
	ZrO_2	0.75	1.31	0.79
5	LiF	1.0	8.26	2.55
	ZrO_2	1.0	1.74	1.05
6	LiF	2.0	15.51	5.01
	ZrO_2	0	0	0
7	LiF	2.0	15.48	5.01
	ZrO_2	0.25	0.41	0.26
8	LiF	2.0	15.45	5.01
	ZrO_2	0.5	0.81	0.52
9	LiF	2.0	15.42	5.01
	ZrO_2	0.75	1.22	0.78
10	LiF	2.0	15.39	5.01
	ZrO_2	1.0	1.62	1.04

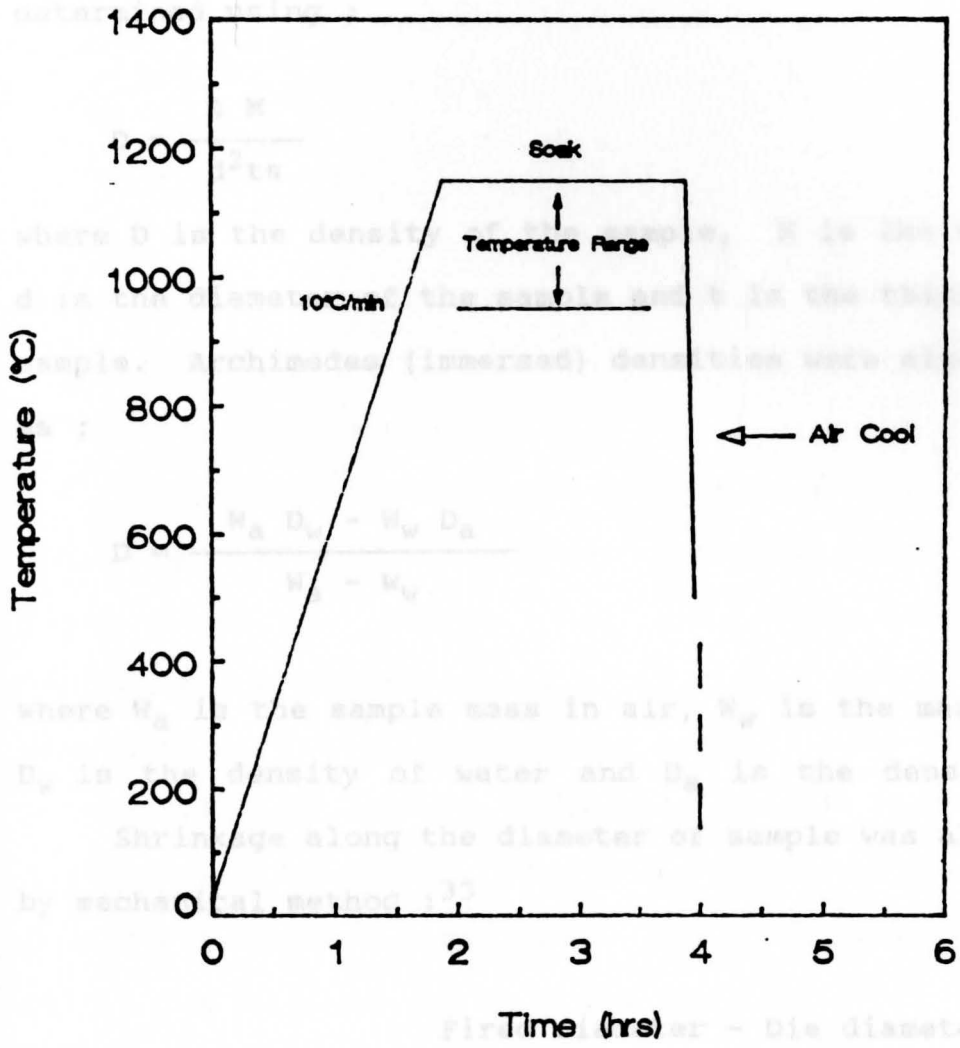

Figure 12. Heating schedule used to sinter fluxed $BaTiO_3$.

3.2. Characterization

Two methods were used to determine the density of sample. The geometric density of as-fired sample was determined using ;

$$D = \frac{4\ M}{d^2 t \pi} \qquad (17)$$

where D is the density of the sample, M is the sample mass, d is the diameter of the sample and t is the thickness of the sample. Archimedes (immersed) densities were also calculated as ;

$$D = \frac{W_a\ D_w - W_w\ D_a}{W_a - W_w} \qquad (18)$$

where W_a is the sample mass in air, W_w is the mass in water, D_w is the density of water and D_a is the density of air.

Shrinkage along the diameter of sample was also measured by mechanical method :[33]

$$\text{Firing shrinkage} = \frac{\text{Fired diameter - Die diameter}}{\text{Die diameter}} \qquad (19)$$

As-sintered surface microstructure was observed using a [Hitachi S-450] Scanning Electron Microscope (SEM). Sintered

samples were mounted on Al stub with colloidal graphite and then coated using an Au sputter [Polaron Instrument Inc.]. The grain sizes were measured from SEM photomicrographs using the line-intercepted method. The grain size was calculated as :[34]

$$G = \frac{1.56\ L}{N\ M} \qquad (20)$$

where G is the average grain diameter, L is the length of the line segment, N is the number of the grain intercepts and M is the magnification.

Some fired compacts were crushed to a fine particle size for X-ray diffraction analysis. The diffraction analysis was performed on the (100) (001) and (200) (002) peaks to determine the axial ratio (c/a) of fluxed $BaTiO_3$. The crystal structure of calcined BaTiO3 powder was found to be tetragonal with lattice parameter (a = 3.9759 Å and c = 4.0198 Å). Therefore, the axial ratio (c/a) of starting powder was found to be 1.011. The lattice parameters were calculated by using the relation given as :[35]

$$\sin^2 \theta = A(h^2 + k^2) + Cl^2 \qquad (21)$$

where $A = \lambda^2/4a^2$ and $C = \lambda^2/4c^2$

h, k, l = Indices

IV. RESULTS AND DISCUSSIONS

4.1. Effect of LiF in Sintered $BaTiO_3$ Ceramics

Pure barium titanate compacts were sintered at temperatures below 1150°C. As discussed in Chapter 1, the normal sintering temperature of $BaTiO_3$ is between 1350°C and 1450°C. Substantial densification of $BaTiO_3$ without LiF did not occur at below 1150°C [Figures 13 (a) and (b)]. SEM photomicrographs in Fig. 13 revealed a porous structure similar to the starting materials. However, Fig. 13(b) showed that small grains were appearing to sinter.

$BaTiO_3$ compacts doped with 1 wt% LiF were sintered at 950°C and 1000°C. Samples were held at the sintering temperature for 0.5, 1 or 2 hr, and then air quenched. A same heat treatment was performed on $BaTiO_3$ compacts doped with 2 wt% LiF. Figures 14 and 15 show densification behavior of LiF fluxed $BaTiO_3$ as a function of sintering time. The maximum density as shown in Fig. 15 was achieved 97% theoretical density (Th.D) with 2 wt% LiF sintered at 1000°C for 2 hr. Compacts with 1 wt% LiF, sintered at 1000°C for 2 hr, resulted in the second highest density (Th.D = 95%). The optimum sintering time (2 hr) was, therefore, chosen as the sintering time for further studies.

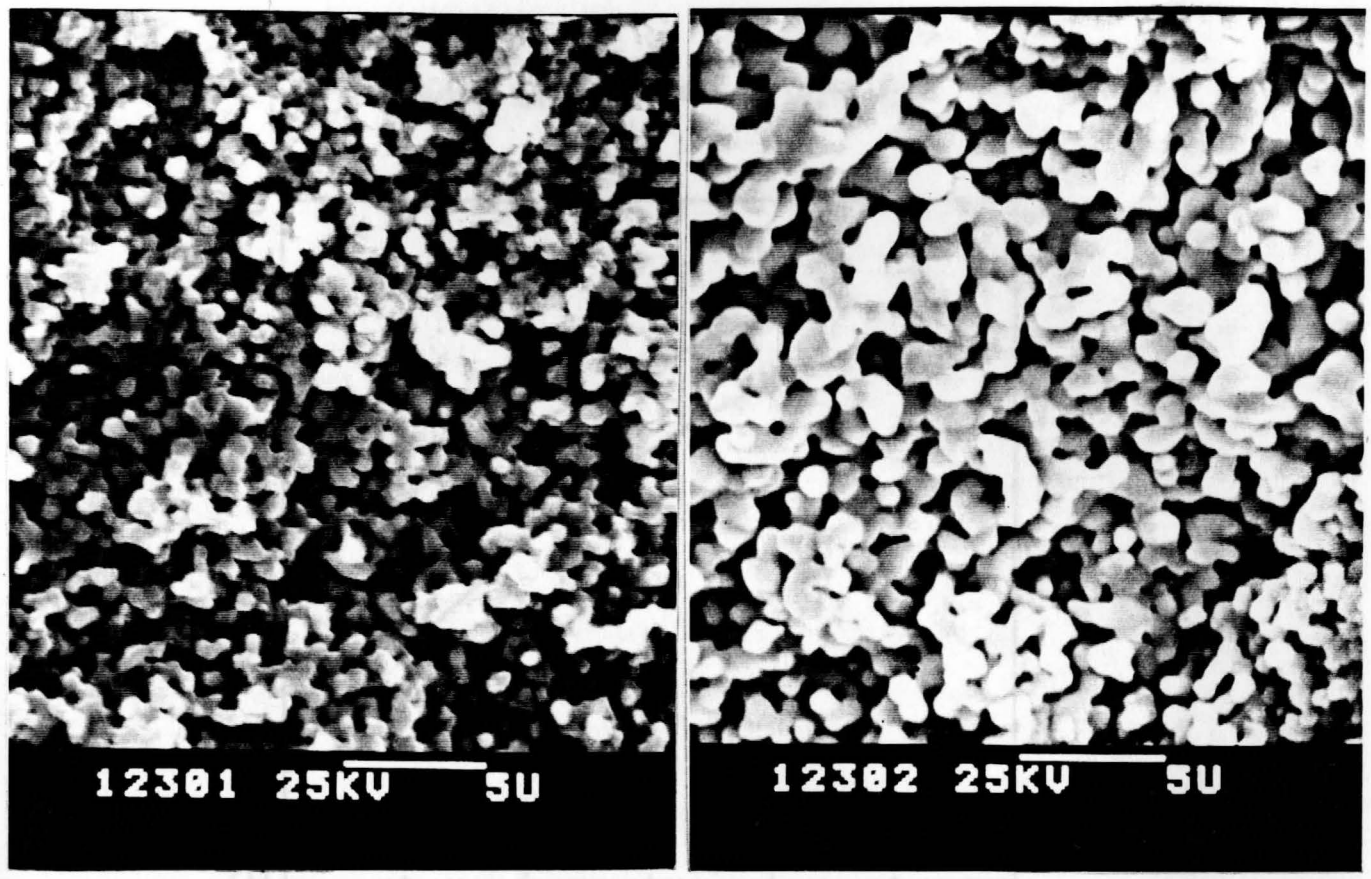

(a) (b)

Figure 13. SEM photographs of pure $BaTiO_3$ (a) sintered at 900°C [X4000] and (b) sintered at 1000°C [X4000, bar = 5 μm].

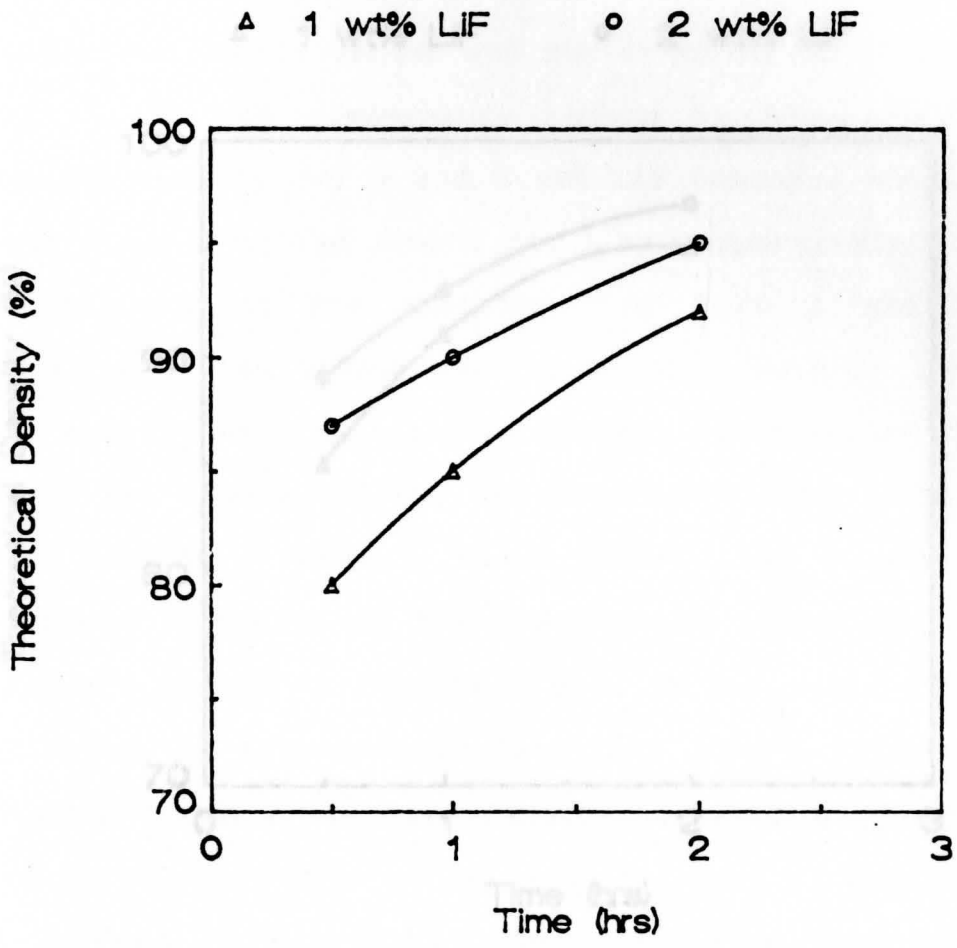

Figure 14. Density as a function of sintering time for $BaTiO_3$ modified with LiF at 950°C.

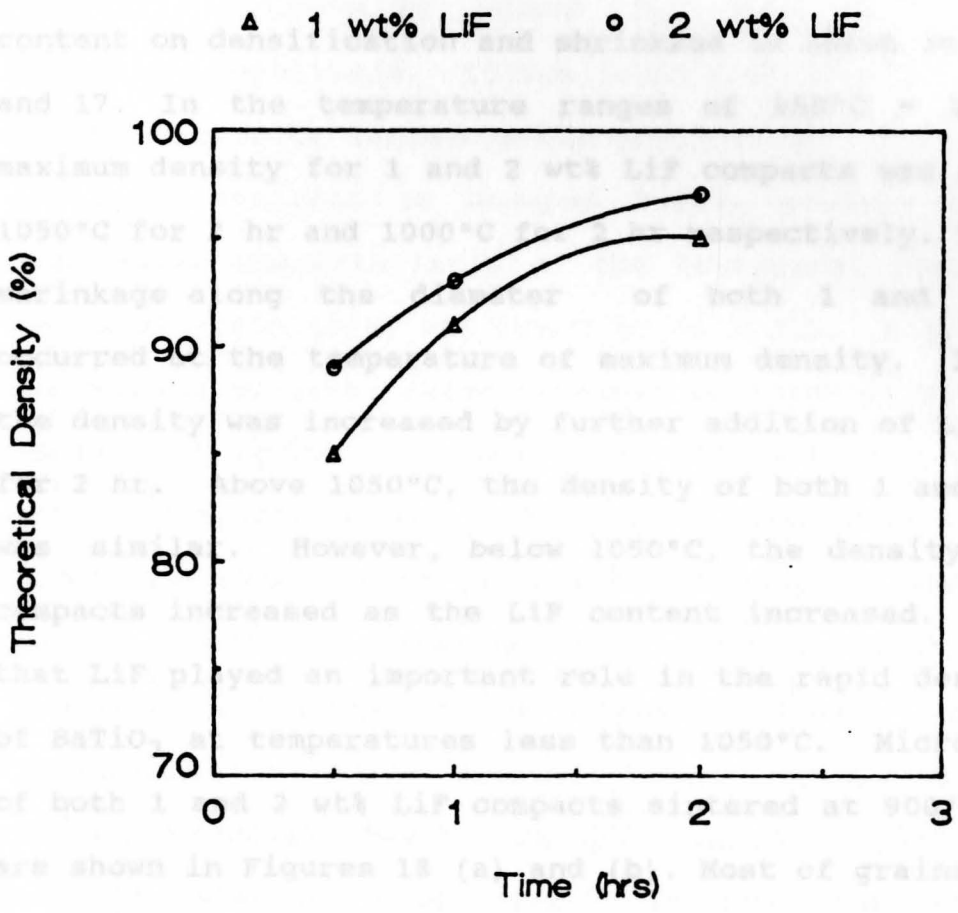

Figure 15. Density as a function of sintering time for $BaTiO_3$ modified with LiF at 1000°C.

At temperatures below 900°C, $BaTiO_3$ compacts with either addition of 1 or 2 wt% LiF required very long sintering times to achieve maximum density of the fired samples. However, densification of the compacts was enhanced as the LiF content increased at temperatures above 950°C. The influence of LiF content on densification and shrinkage is shown in Figures 16 and 17. In the temperature ranges of 950°C - 1050°C, the maximum density for 1 and 2 wt% LiF compacts was achieved at 1050°C for 2 hr and 1000°C for 2 hr respectively. The maximum shrinkage along the diameter of both 1 and 2 wt% LiF occurred at the temperature of maximum density. In Fig. 16, the density was increased by further addition of LiF at 950°C for 2 hr. Above 1050°C, the density of both 1 and 2 wt% LiF was similar. However, below 1050°C, the density of $BaTiO_3$ compacts increased as the LiF content increased. It seemed that LiF played an important role in the rapid densification of $BaTiO_3$ at temperatures less than 1050°C. Microstructures of both 1 and 2 wt% LiF compacts sintered at 900°C for 2 hr are shown in Figures 18 (a) and (b). Most of grains are cubic in habitat [Fig. 18(a)]. This indicates that liquid phase transport takes place during sintering. A liquid phase was observed in the microstructure of 2 wt% LiF compact sintered at 900°C for 2 hr [Fig.18(b)]. Average grain size (AGS) of both 1 and 2 wt% LiF compacts sintered at 900°C for 2 hr is

about 3 - 5 μm and 7 -10 μm respectively. This indicates that a liquid phase in the microstructure leads to bigger grains. Above 900°C, grain size became larger as LiF content increased. Microstructure of 2 wt% LiF compact sintered at 1050°C for 2 hr showed almost bimodal structure (AGS $\approx$ 18 μm) [Fig. 19]. Figure 20 shows grain size as a function of sintering temperature. It was found that the LiF content was the key factor to influence the grain size.

X-ray analysis of undoped $BaTiO_3$ powders showed only those peaks characteristic of the tetragonal phase at 25°C. Its axial ratio (c/a) was found to be 1.011. Figure 21 shows the results of axial ratio obtained by x-ray diffraction as a function of sintering temperature. Above 800°C, both 1 and 2 wt% LiF compacts became tetragonal to pseudocubic perovskite phase. The axial ratio of 2 wt% LiF samples was less than that of 1 wt% LiF compacts. This indicates that increasing amounts of LiF suppress the tetragonal phase above 800°C. The pseudocubic phase appeared more rapidly as the LiF content increased. Based upon X-ray analysis, $BaTiO_3$ compact with LiF undergoes phase transformations from tetragonal to pseudocubic to tetragonal structure.

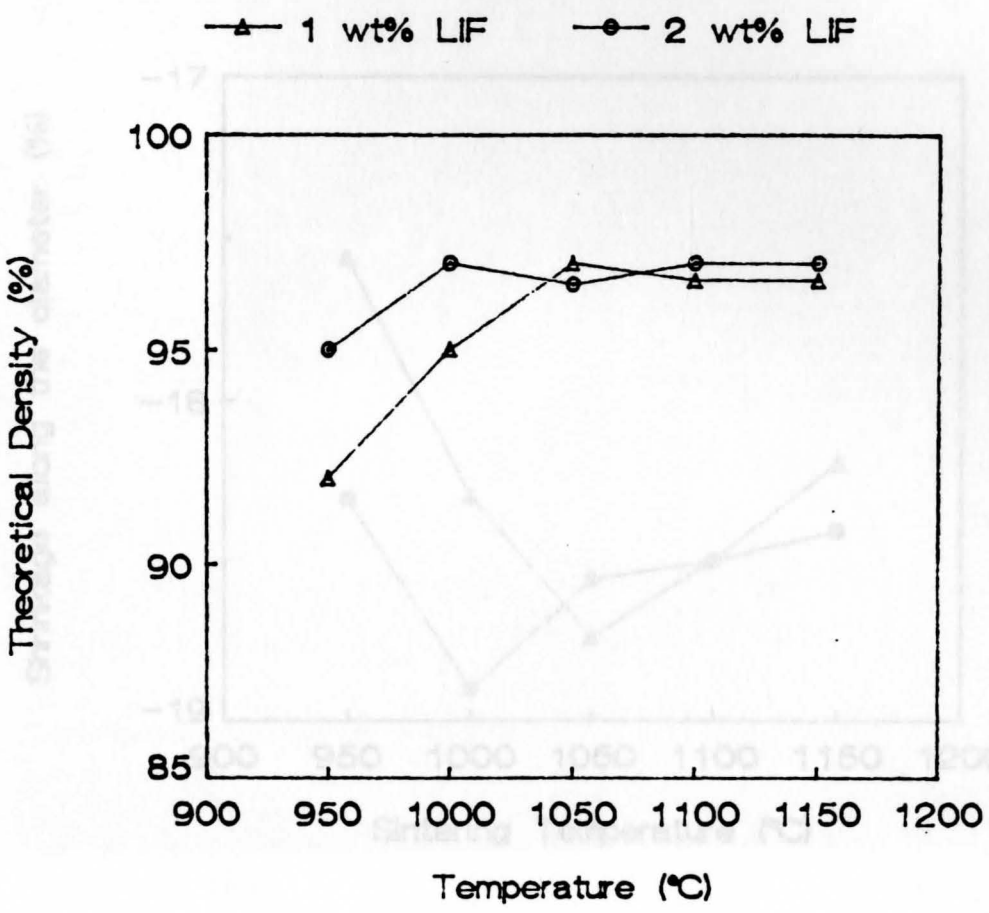

Figure 16. Density as a function of sintering temperature for LiF fluxed $BaTiO_3$ compact.

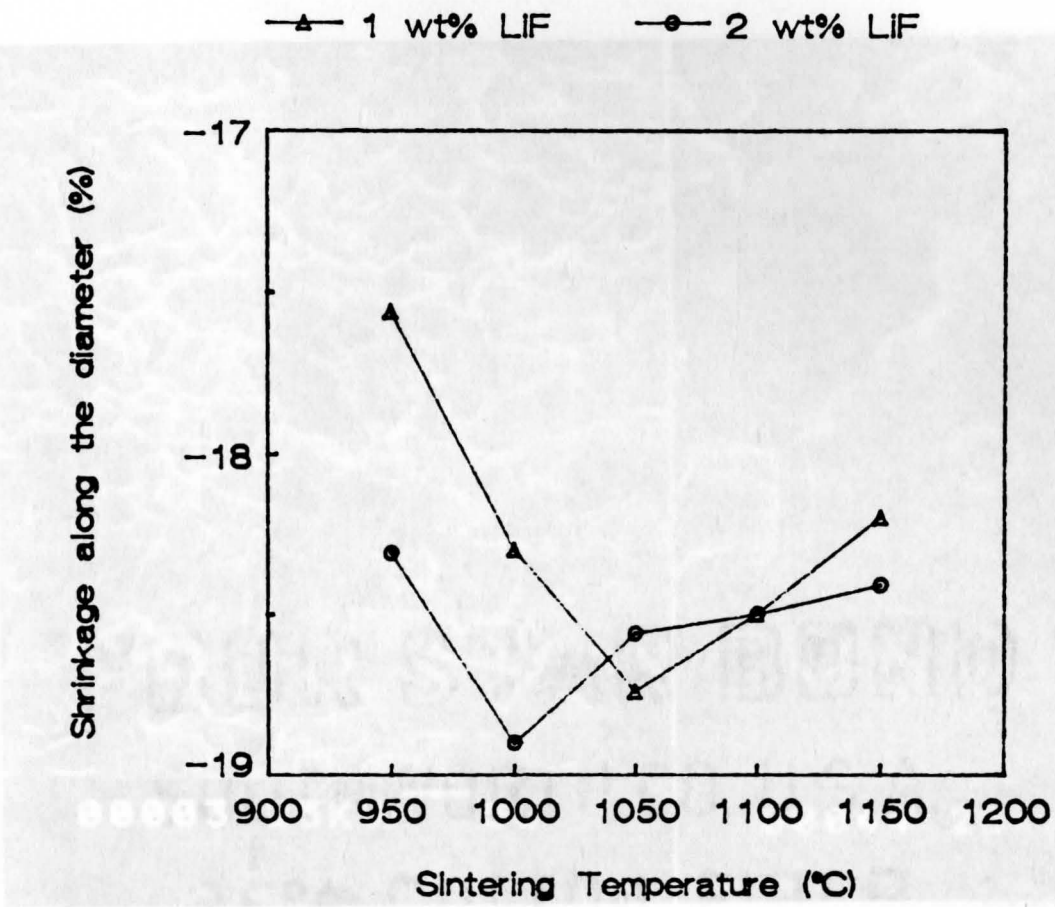

Figure 17. Firing shrinkage along the diameter as a function of sintering temperature for LiF fluxed $BaTiO_3$.

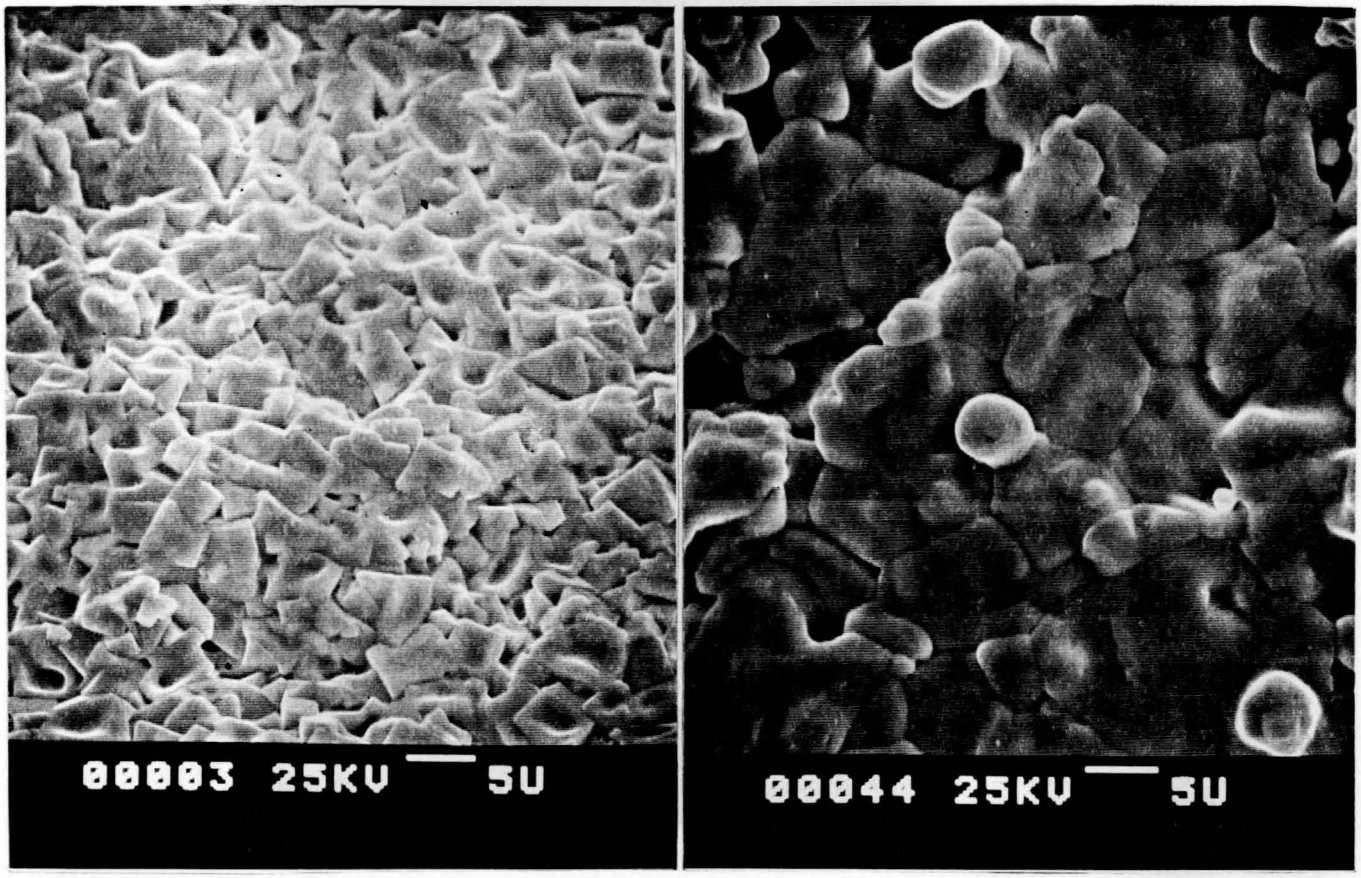

(a) (b)

Figure 18. SEM photographs of as-sintered $BaTiO_3$ at 900°C for 2 hr (a) with 1 wt% LiF and (b) 2 wt% LiF, [X2000, bar = 5 μm].

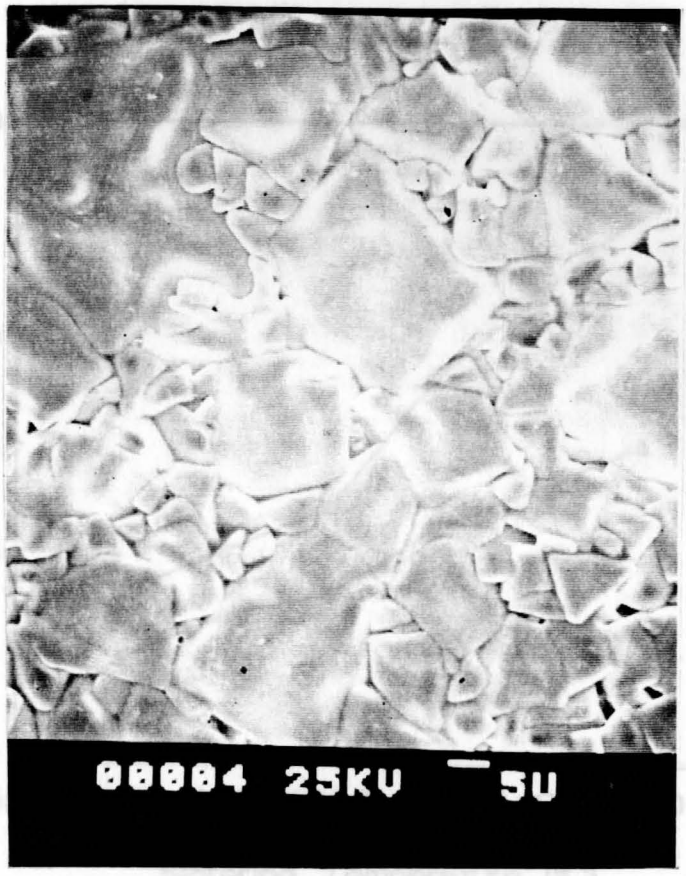

Figure 19. SEM photograph of as-sintered 2 wt% LiF fluxed $BaTiO_3$ at 1050°C for 2hr, [X1000, bar = 5 μm].

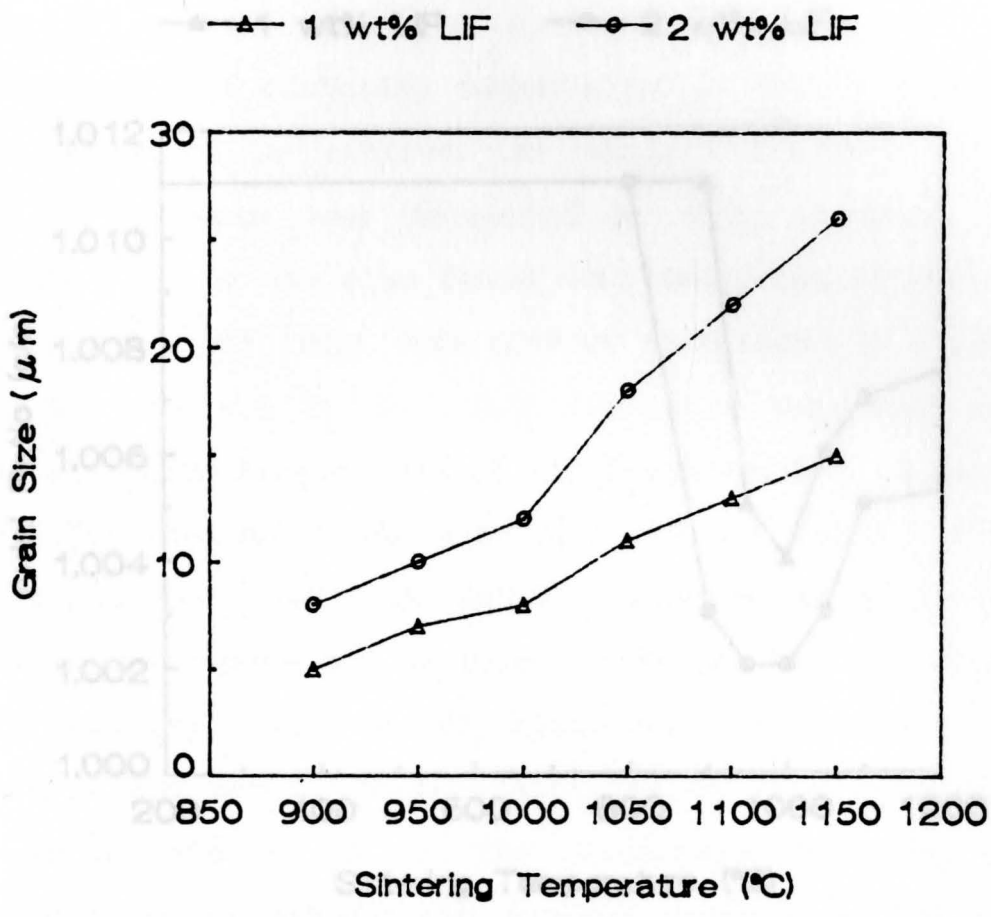

Figure 20. Grain size as a function of sintering temperature for $BaTiO_3$ with LiF addition.

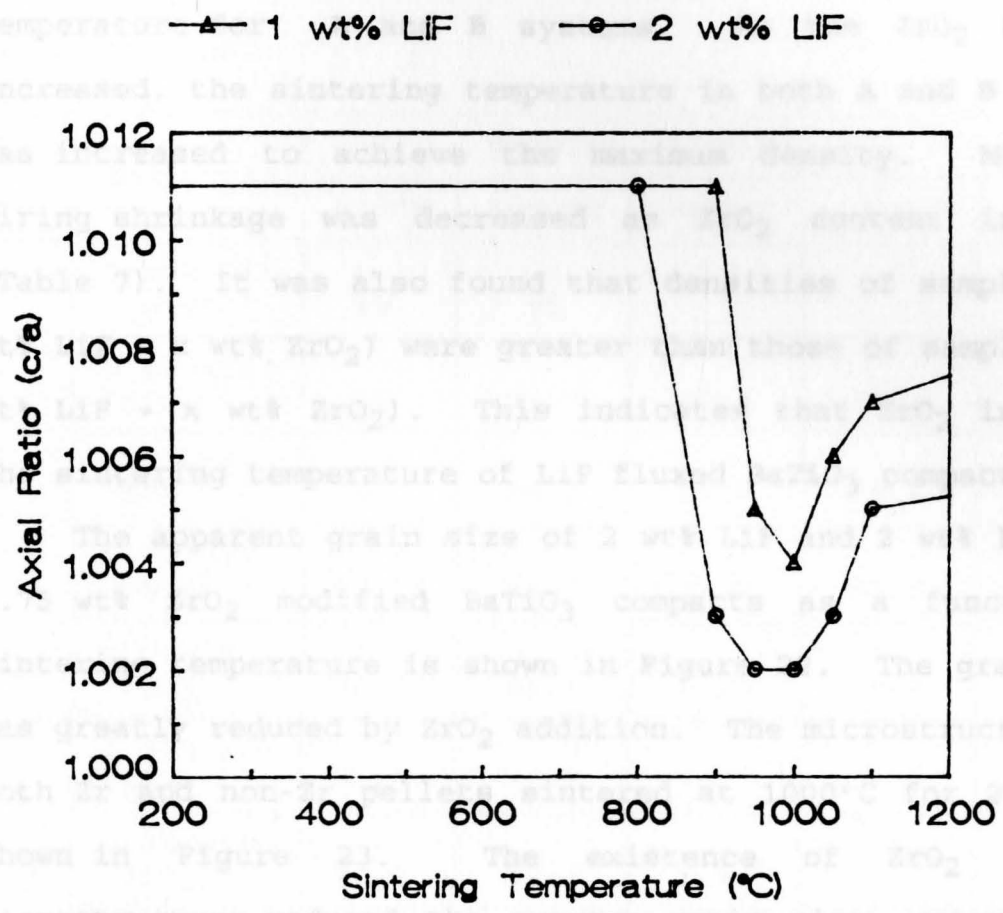

Figure 21. The axial ratio (c/a) as a function of sintering temperature for $BaTiO_3$ with LiF addition.

4.2. Effects of ZrO_2 in LiF fluxed $BaTiO_3$ Ceramics

Unstabilized ZrO_2 (0 - 1 wt%) was added to 1 and 2 wt% LiF fluxed $BaTiO_3$, labeled **A** and **B** respectively. Table 6 gives compositon and density data as a function of sintering temperature for **A** and **B** systems. As the ZrO_2 addition increased, the sintering temperature in both **A** and **B** systems was increased to achieve the maximum density. Moreover, firing shrinkage was decreased as ZrO_2 content increased (Table 7). It was also found that densities of samples **B** (2 wt% LiF + x wt% ZrO_2) were greater than those of samples **A** (1 wt% LiF + x wt% ZrO_2). This indicates that ZrO_2 increases the sintering temperature of LiF fluxed $BaTiO_3$ compacts.

The apparent grain size of 2 wt% LiF and 2 wt% LiF plus 0.75 wt% ZrO_2 modified $BaTiO_3$ compacts as a function of sintering temperature is shown in Figure 22. The grain size was greatly reduced by ZrO_2 addition. The microstructures of both Zr and non-Zr pellets sintered at 1000°C for 2 hr are shown in Figure 23. The existence of ZrO_2 in the microstructure reduced the average grain size, retarded the exaggerated grain growth and became a more uniform microstructure. In Figure 24(a), a bimodal microstructure (AGS ≈ 12 μm) for 2 wt% LiF fluxed without ZrO_2 sample sintered at 1000°C for 2 hr is shown. Added ZrO_2 gradually suppressed the bimodal grain growth and reduced the grain

Table 6. Densities of fluxed-sintered $BaTiO_3$ as a function of added ZrO_2 concentration at different sintering temperatures held for 2 hr.

	Additives	Density (% Th.D)				
		950°C	1000°C	1050°C	1100°C	1150°C
A	1 wt% LiF plus	90	> 95			
	0.25 wt% ZrO_2	91	91.3	90.3	92.4	93.6
	0.5 wt% ZrO_2	81	90.2	89.7	86.4	90.8
	0.75 wt% ZrO_2	82.1	86.2	74.2	83.5	93.3
	1.0 wt% ZrO_2	80.1	81.4	69.7	78.8	87.8
B	2 wt% LiF plus	> 95				
	0.25 wt% ZrO_2	97.4	97.8	> 97		
	0.5 wt% ZrO_2	95.4	97.5	97.1	93.1	95.0
	0.75 wt% ZrO_2	89.7	89.7	87.7	81.9	84.4
	1.0 wt% ZrO_2	88.6	84.9	84.4	85.4	80.8

Table 7. Firing shrinkage along the diameter at various sintering temperatures held for 2 hr.

	Additives	Shrinkage (%)				
		950°C	1000°C	1050°C	1100°C	1150°C
A	1 wt% LiF plus	-17.56	- 18.3	-18.74	-18.5	-18.2
	0.25 wt% ZrO_2	-18.90	-18.89	-17.32	-17.32	-17.52
	0.5 wt% ZrO_2	-15.75	-16.14	-16.54	-15.35	-15.75
	0.75 wt% ZrO_2	-12.99	-16.54	-10.94	-12.6	-13.78
	1.0 wt% ZrO_2	-12.99	-11.61	-12.60	-10.63	-12.80
B	2 wt% LiF plus	-18.31	-18.90	-18.56	-18.5	-18.41
	0.25 wt% ZrO_2	-17.26	-17.20	-17.11	-17.50	-17.56
	0.5 wt% ZrO_2	-17.24	-16.93	-16.14	-16.54	-15.75
	0.75 wt% ZrO_2	-14.17	-15.35	-14.96	-13.98	-13.39
	1.0 wt% ZrO_2	-15.75	-14.57	-14.76	-13.39	-13.39

size (AGS ≈ 5 μm), [Fig. 24(b)]. A uniform grained (AGS ≈ 2 μm) microstructure with 0.75 wt% ZrO_2 plus 2 wt% LiF added compact sintered at 1050°C for 2 hr is shown in Figure 24(c). A similar progression is found with the 1 wt% LiF fluxed compacts which again show [Fig. 25(a)] a bimodal microstructure (AGS ≈ 5 μm) with 0.25 wt% ZrO_2. With 0.5 wt% added ZrO_2, the grain growth was suppressed [Fig. 25(b)] and grains became the sphere in habitat. This indicates that Zr^{4+} ions diffuse into the $BaTiO_3$ lattice, resulting in inhibiting the grain growth. Figure 25(c) shows a uniform microstructure with 0.75 wt% ZrO_2 sintered at 950°C for 2 hr. The microstructure of Fig. 25(c) was found to be porous and a liquid phase was observed. This confirms again that ZrO_2 increases the sintering temperature of $BaTiO_3$ compact. Figures 26 - 30 show the variation of the grain size of sintered compacts with the composition of ZrO_2 at the sintering temperatures. It was found that, with ZrO_2 addition, the grain size of 1 wt% LiF fluxed compacts was smaller than that of 2 wt% LiF fluxed compacts.

X-ray analysis of ZrO_2 additions to LiF fluxed $BaTiO_3$ shows suppression of the tetragonal structure in favor of a more cubic modification, [Table 8]. Without ZrO_2, LiF fluxed $BaTiO_3$ compacts undergo the phase transformation from tetragonal to cubic to tetragonal. However, further

additions of ZrO_2 in LiF fluxed $BaTiO_3$ compact result in a pseudocubic perovskite phase.

Table 8. Effect of ZrO_2 on the axial ratio of $BaTiO_3$.

Sample	Sint.temp.(°C)	c/a	Phase
$BaTiO_3$		1.011	tetragonal
Plus 1 wt% LiF	1150	1.008	tetragonal
Plus ZrO_2 (wt%)			
0.25	1100	1.008	tetragonal
0.5	1100	1.007	tetragonal
0.5	1150	1.006	tetragonal
0.75	1100	1.005	tetragonal
1.0	1150	1.003	pseudocubic
Plus 2 wt% LiF	1150	1.006	tetragonal
Plus ZrO_2 (wt%)			
0.25	1050	1.006	tetragonal
0.25	1150	1.005	tetragonal
0.5	1150	1.003	pseudocubic
0.75	1100	≈ 1	pure cubic
1.0	1100	≈ 1	pure cubic

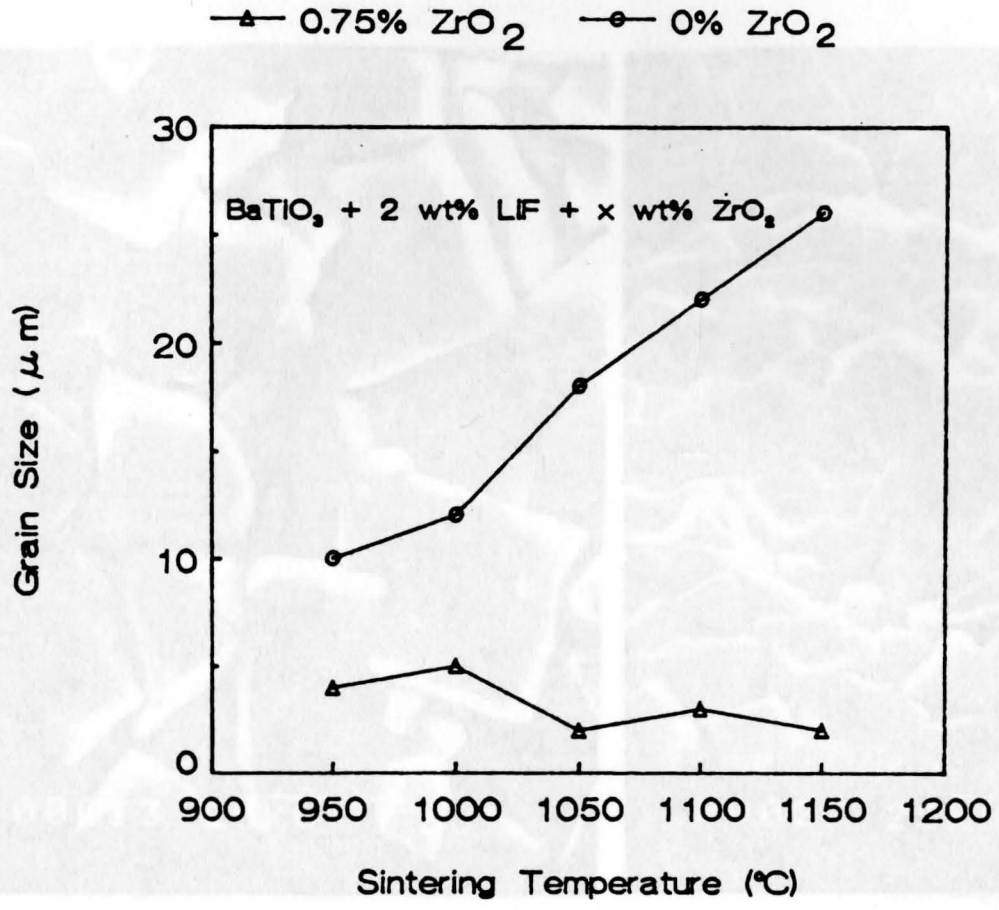

Figure 22. Grain size as a function of sintering temperature of 2 wt% LiF fluxed $BaTiO_3$ with ZrO_2 or without ZrO_2.

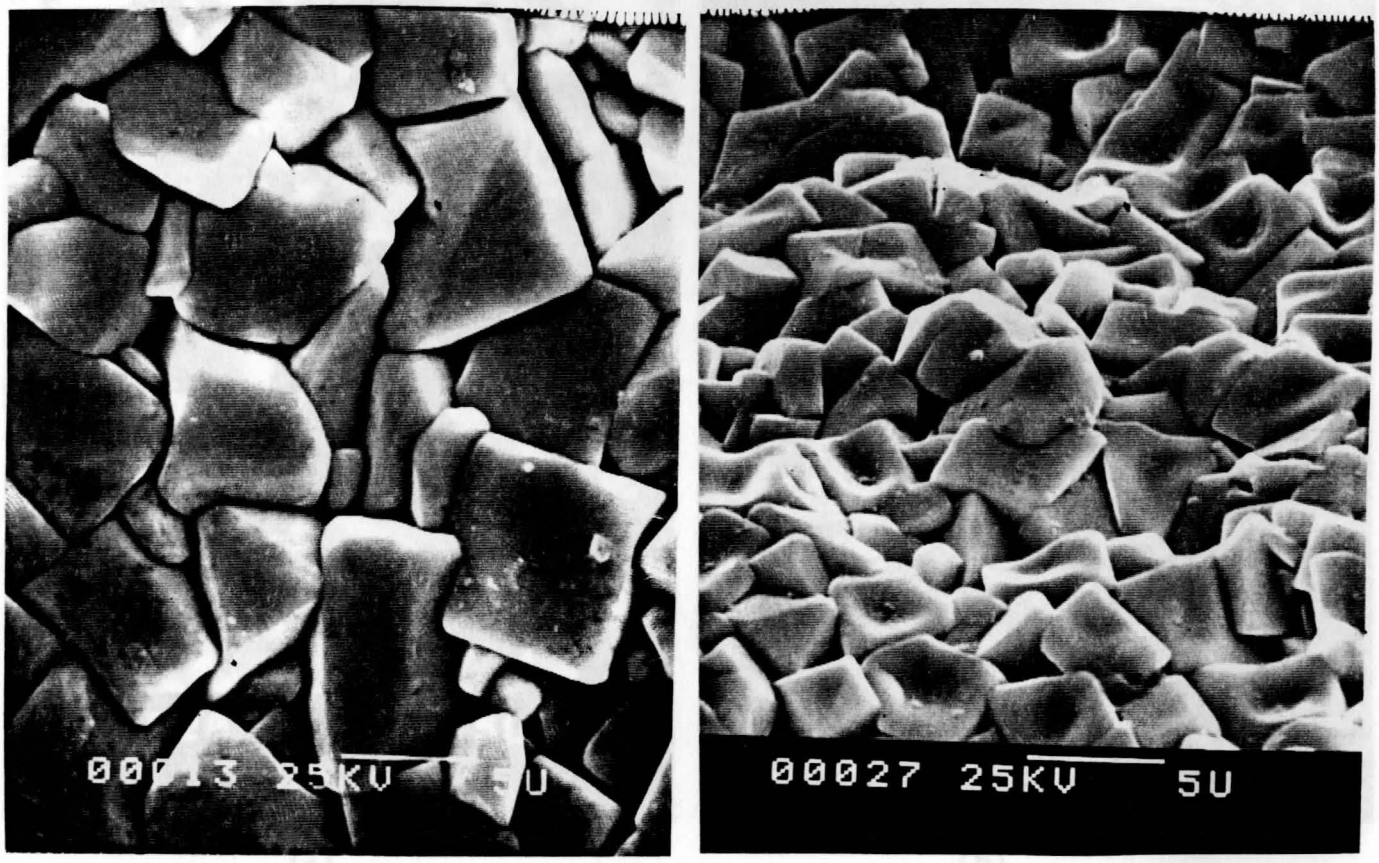

(a) (b)

Figure 23. SEM photographs of as-sintered surfaces of $BaTiO_3$ modified with (a) 1 wt% LiF without ZrO_2 (1000°C) and (b) 1 wt% LiF plus 0.25 wt% ZrO_2 (1000°C); soaked for 2 hr [X4000, bar = 5 μm].

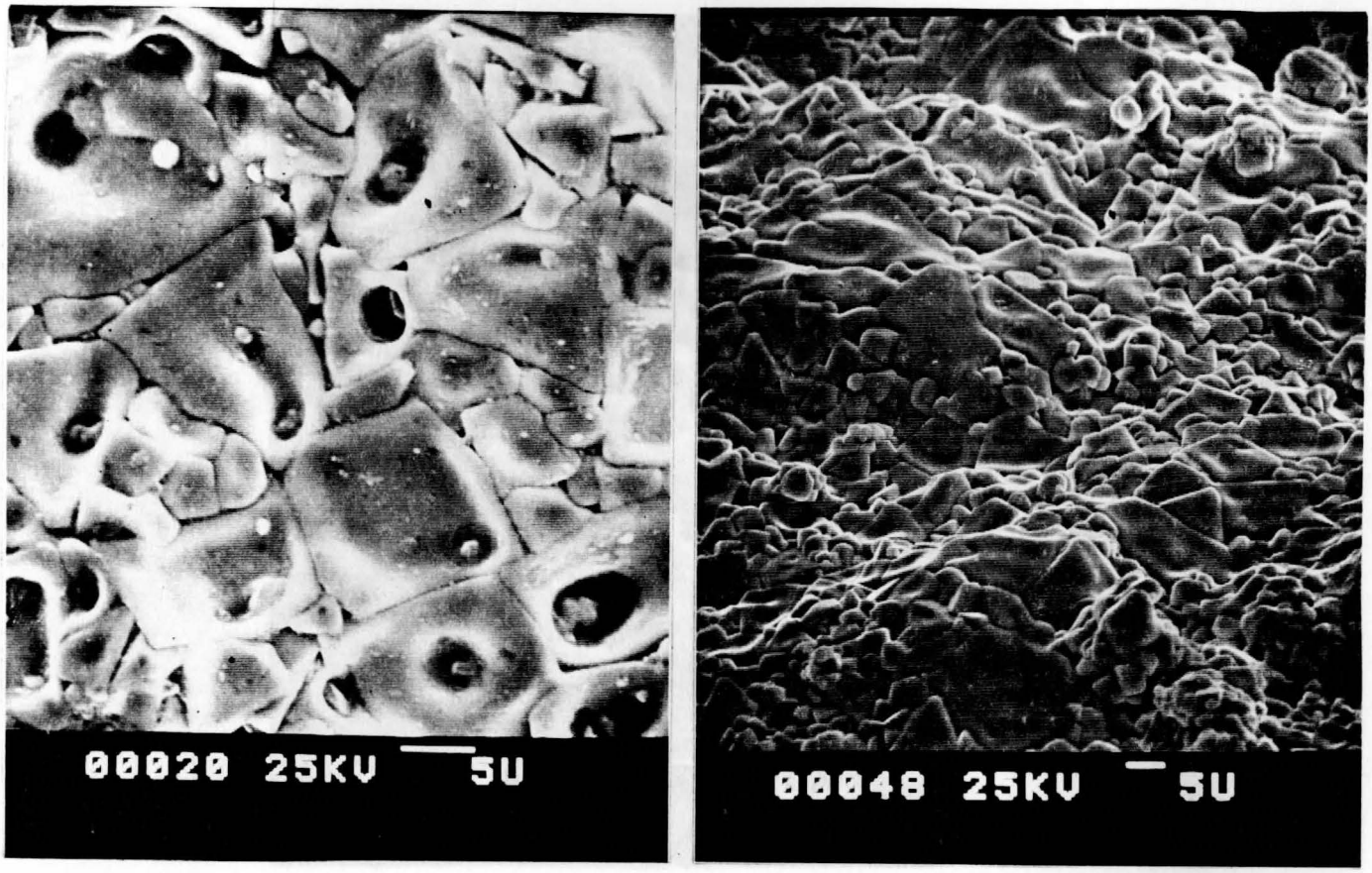

(a) (b)

Figure 24. SEM images of as-sintered surfaces of $BaTiO_3$ modified with (a) 2 wt% LiF (1000°C) and (b) plus 0.5 wt% added ZrO_2 (1050°C); soaked for 2 hr, [bar = 5 μm].

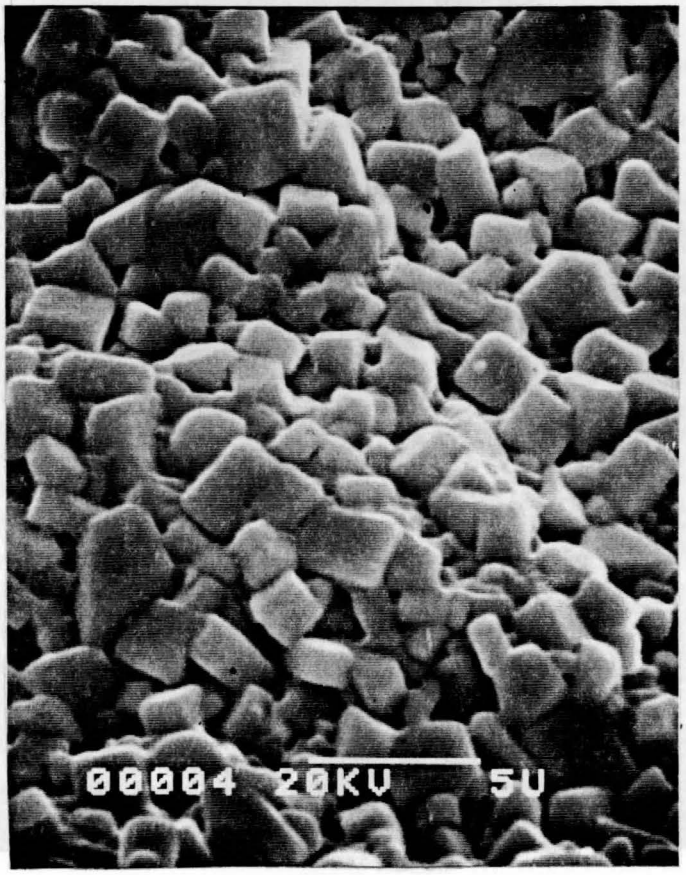

(c)

Figure 24(c). SEM photograph of as-sintered surface of $BaTiO_3$ with 2 wt% LiF plus 0.75 wt% added ZrO_2 (1050°C) soaked for 2 hr, [bar = 5 μm].

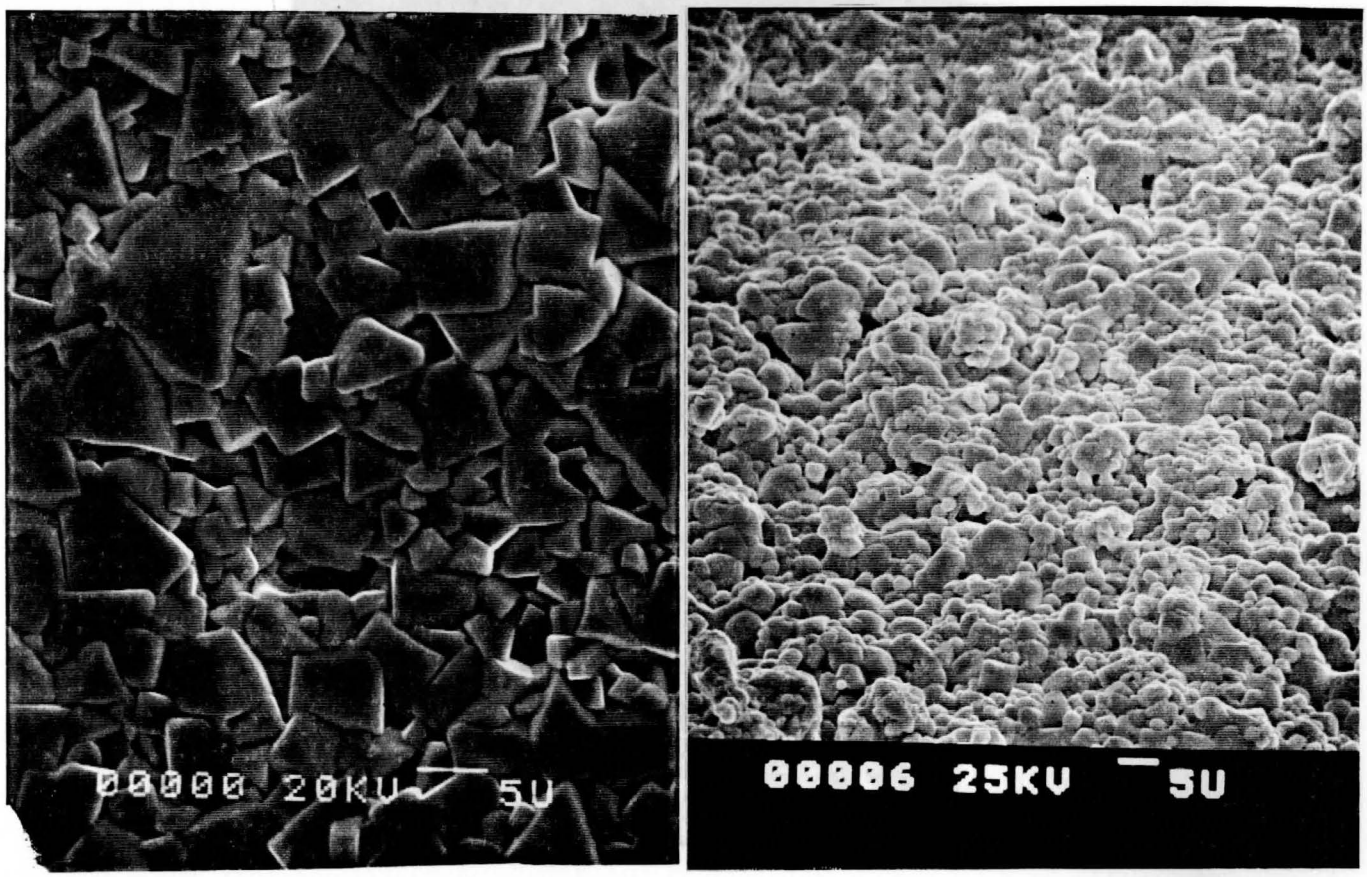

(a) (b)

Figure 25. SEM images of as-sintered surfaces of $BaTiO_3$ with (a) 1 wt% LiF (950°C) and (b) plus 0.5 wt% added ZrO_2 (950°C) soaked for 2 hr, [bar = 5 μm].

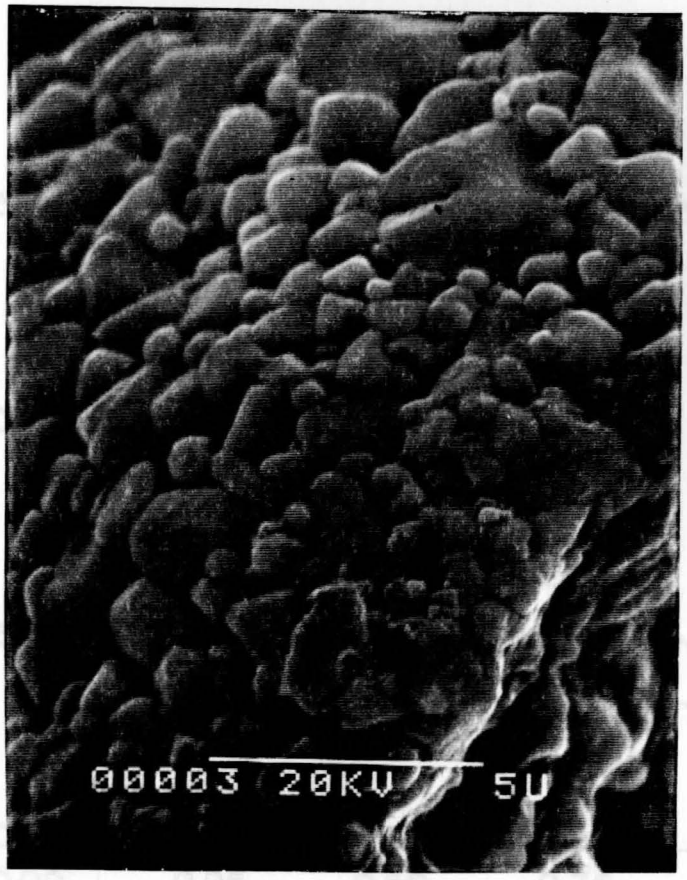

(c)

Figure 25(c). SEM image of as-sintered of $BaTiO_3$ with 1 wt% LiF plus 0.75 wt% ZrO_2 (950°C) soaked for 2 hr, [bar = 5 μm].

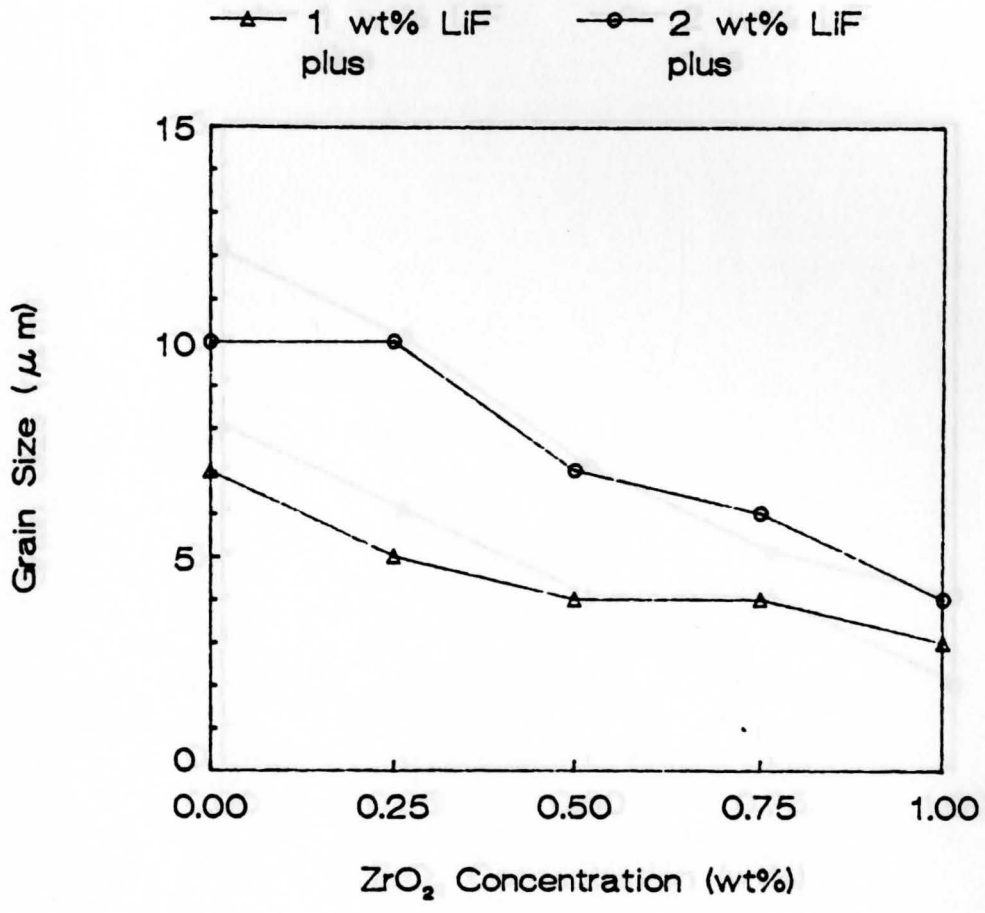

Figure 26. Grain size as a function of added ZrO_2 concentration at 950°C for 2 hr.

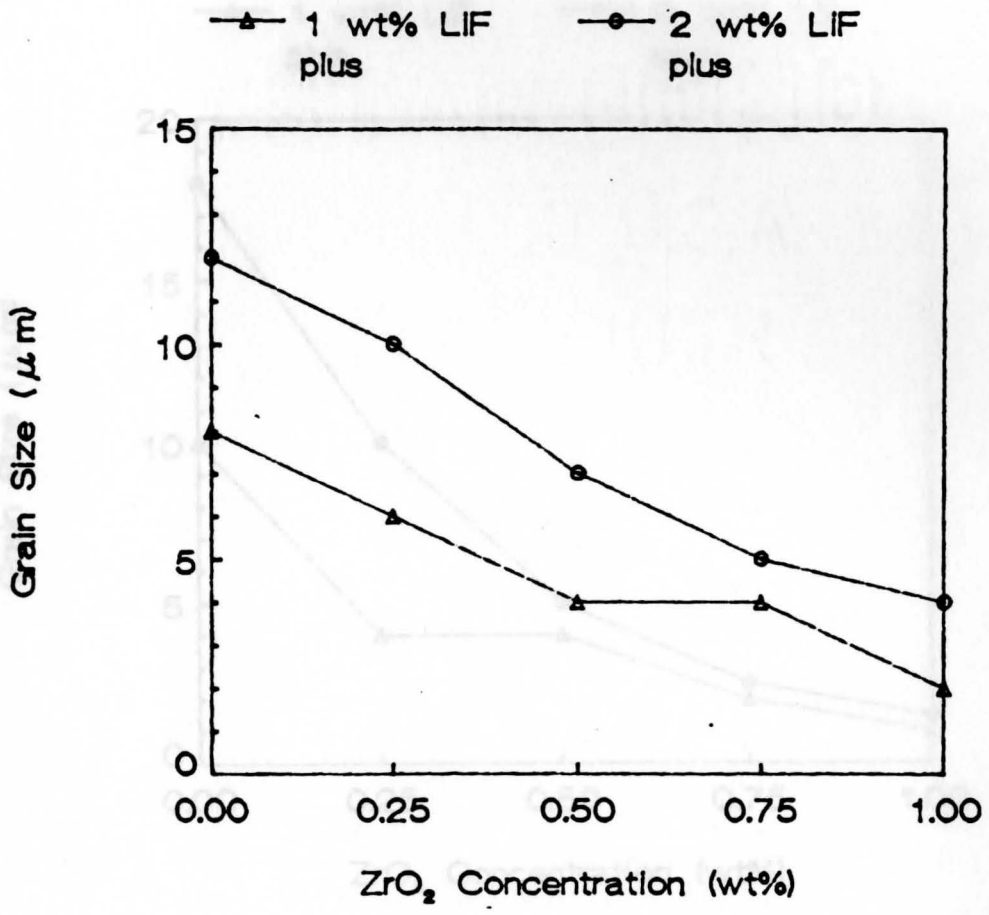

Figure 27. Grain size as a function of added ZrO_2 concentration at 1000°C for 2 hr.

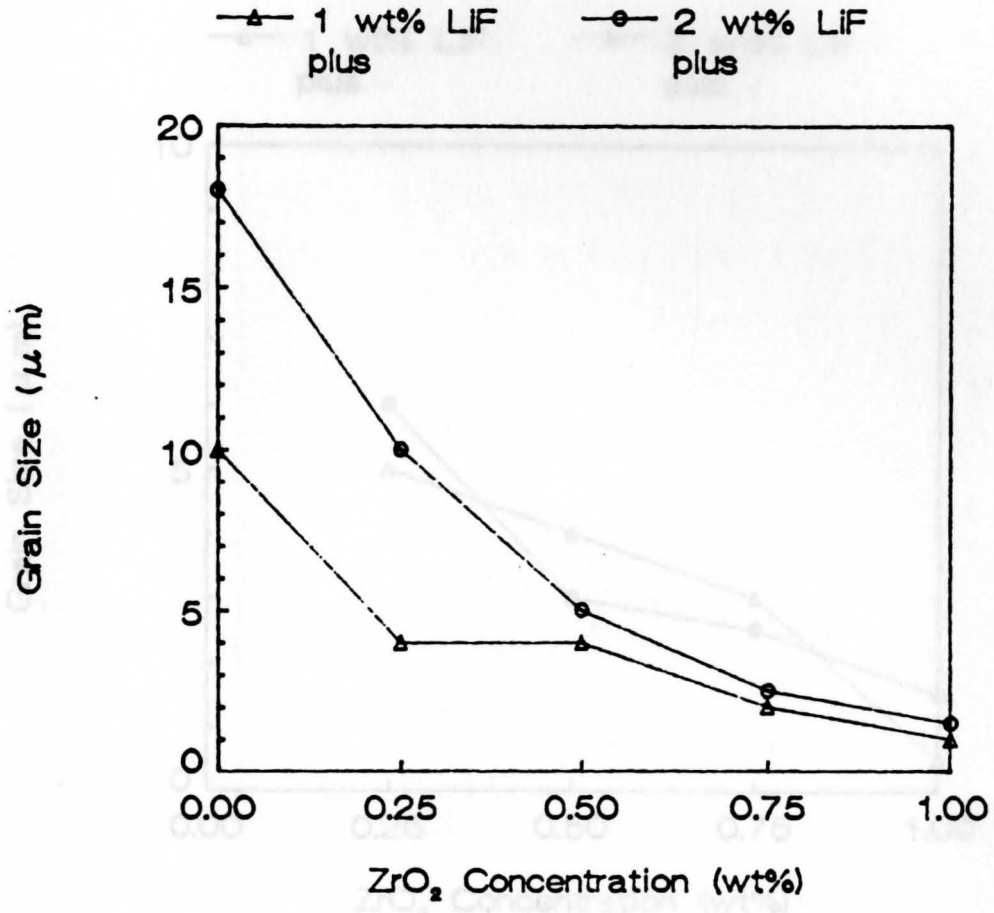

Figure 28. Grain size as a function of added ZrO_2 concentration at 1050°C for 2 hr.

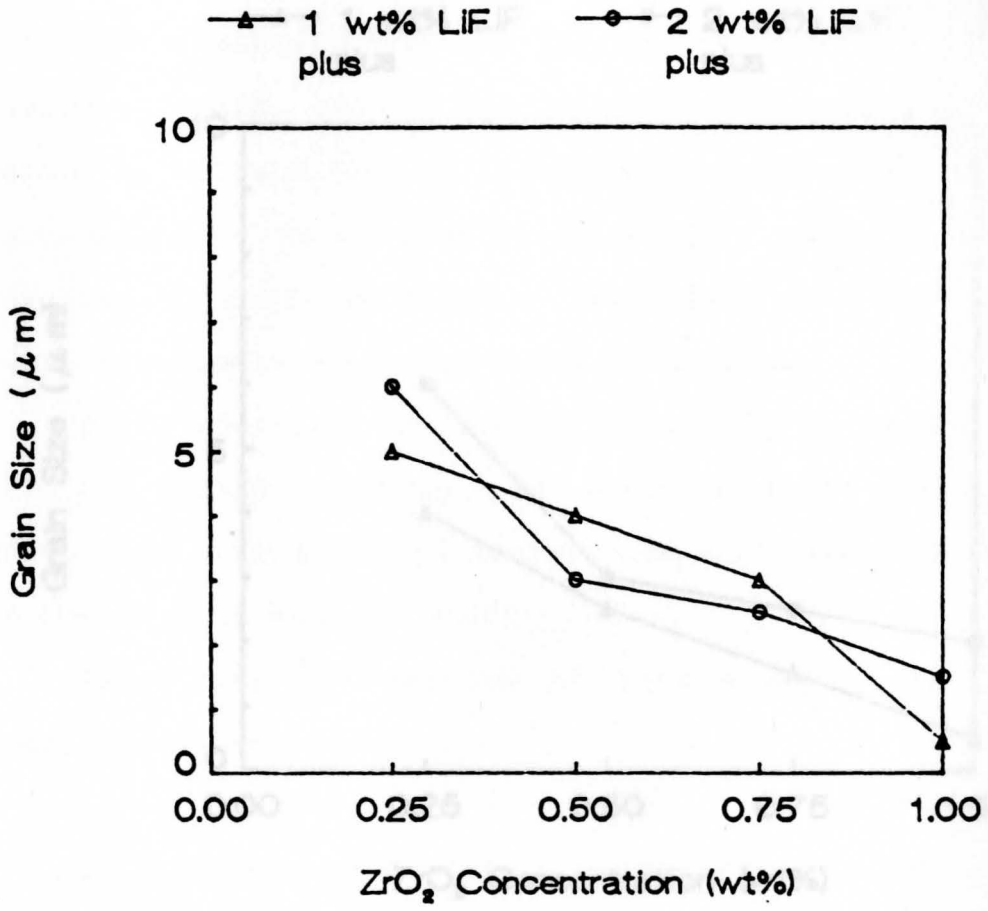

Figure 29. Grain size as a function of added ZrO_2 concentration at 1100°C for 2 hr.

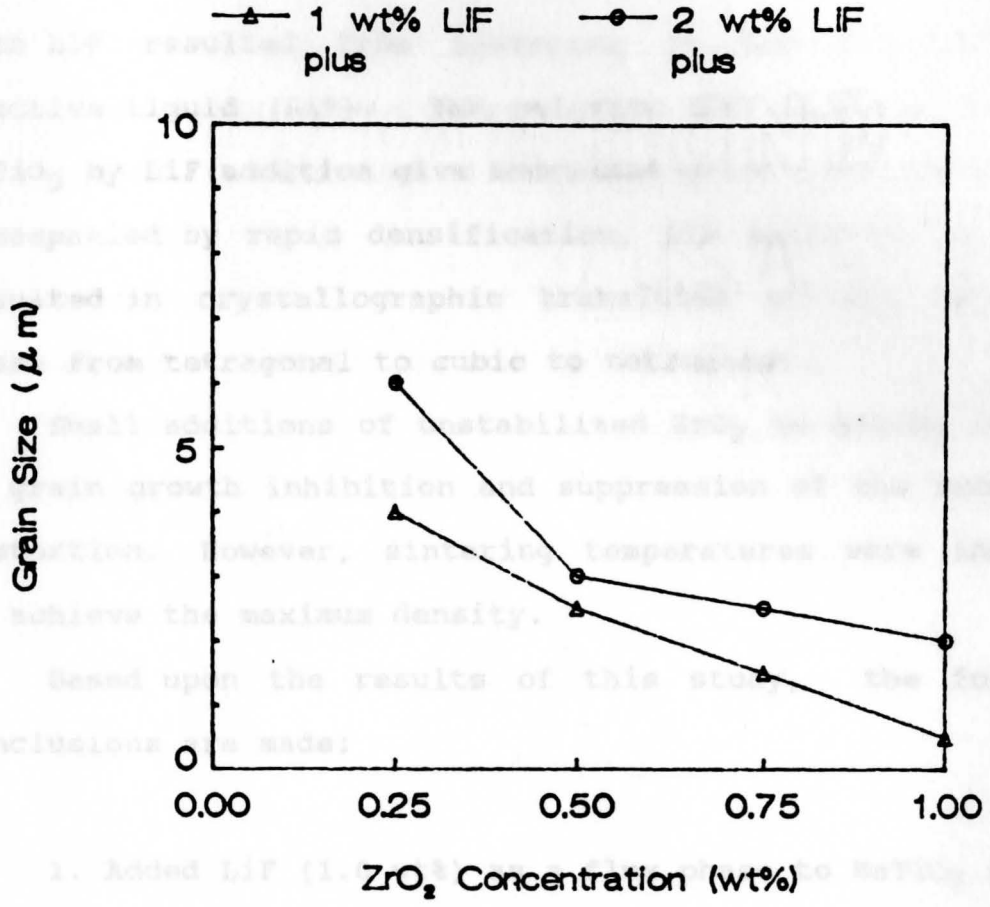

Figure 30. Grain size as a function of added ZrO_2 concentration at 1150°C for 2 hr.

V. SUMMARY AND CONCLUSION

In summary, this work has shown that small amounts of LiF flux additions to $BaTiO_3$ can significantly reduce the sintering temperature. The rapid densification of $BaTiO_3$ with LiF resulted from sintering in the presence of a reactive liquid (LiF). The solution and reprecipitation of $BaTiO_3$ by LiF addition give increased grain size and density. Accompanied by rapid densification, LiF additions to $BaTiO_3$ resulted in crystallographic transition of the perovskite phase from tetragonal to cubic to tetragonal.

Small additions of unstabilized ZrO_2 to $BaTiO_3$ resulted in grain growth inhibition and suppression of the tetragonal distortion. However, sintering temperatures were increased to achieve the maximum density.

Based upon the results of this study, the following conclusions are made:

1. Added LiF (1.0 wt%) as a flux phase to $BaTiO_3$ reduced the sintering temperature to $\leq$ 1100°C.

2. Further addition of LiF (2.0 wt%) resulted in a larger grain size and pseudocubic phase.

3. Additions of ZrO_2, as little as 0.25 wt%, to the flux phase reduce the diffusion of the flux agent (LiF) into $BaTiO_3$. Therefore, the sintering temperatures were increased to achieve the maximum density.

4. The existence of ZrO_2 at the grain boundaries resulted in suppression of grain growth and finally led to the uniform and fine microstructure.

5. Further additions of ZrO_2 ($\leq$1.0 wt%) to the fluxed $BaTiO_3$ led to smaller grain size ($\leq$1.0 μm), a pure cubic phase, higher sintering temperature and more uniform microstructure.

REFERENCES

1. D. HENNINGS, "Liquid Phase Sintering of Barium Titanate", Ber. Dt. Keram. Ges., Vol.55 [7] 359 - 60 (1978).
2. W.D. KINGERY, Introduction to Ceramics, JONE WILEY & SON, INC., CHAPTS 13, 20, (1969).
3. S.L. FU, C.C. WEI, S.Y. CHENG, and T.P. YEH, "Low Temperature Firing of Ceramics", ISHM **8** [1] 1 - 5 (1985)
4. W.R. BUESSEM and T.I. PROKOPOWICZ, "Electrode and Materials Problems in Ceramic Capacitors", Ferroelectrics, [10], 225 - 30, (1976).
5. S.J. JANG, W.A. SCHULZE and J.V. BIGGERS, "Low Firing Capacitor Dielectrics in the System $Pb(Fe_{2/3}W_{1/3})O_3 \cdot Pb(Fe_{1/2}Nb_{1/2})O_3 \cdot Pb_5Ge_3O_{11}$", Am. Ceram. Soc. Bull., **62** [2] 216 - 18 (1983).
6. T.R.AMSTRONG, K.A. YOUNG and R.C. BUCHANAN, "Dielectric Properties of Fluxed Barium Titanate Ceramics with Zirconia Additions", J. Am. Ceram. Soc., **73** [3] 700 -706, (1990).
7. IAN BURN, "Flux-Sintered $BaTiO_3$ Dielectrics", J. Matls. Sci., **17**, 1398 -1408 (1982).
8. J.M. HAUSSONE, G. GESGARDIN, P.H. BAJOLET, and B. RAVEAN, "Barium Titanate Sintered With LiF", J. Am. Ceram. Soc., **66** [11] 801 - 807 (1983).

9. B.E. WALKER, R.W. RICE, R.C. POHANKA, and J.R. SPAMN, "Densification and Strength of $BaTiO_3$ with LiF and MgO Additives", Am. Ceram. Bull., Vol.55, [5] 274 - 85 (1971).

10. L.M. CASTELLIZE and R.J. ROUTIL, "The Effect of Boric oxide on the Properties of Barium Titanate Based Ceramics", J. Can. Ceram. Soc., **35,** 69 - 74, (1969).

11. T.R. AMSTRONG, L.E. MORGENS, A.K. MAURICE, and R.C. BUCHANAN, "The Effects of Zirconia on the Microstructure and Dielectric Properties of Barium Titanate Ceramics", J. Am. Ceram. Soc., Vol.72, [4], 605 - 11 (1989).

12. L.H. VAN VLACK, Physical Ceramics for Engineer, Addision-Wesley Publishing Inc., Chpt.10, (1964).

13. A.J. DEKKER, Electrical Engineering Materials, Prentice Hall, Chpt.2,3 (1989).

14. B. JAFFE, W.R. COOK, and H. JAFFE, Piezoelectric Ceramics Academic Press, 315pp (1971).

15. H.U. ANDERSON, "Influence of Ba/Ti Ratio on the Initial Sintering Kinetics of $BaTiO_3$", J. Am. Ceram. Soc., Vol.56 [11], 605 - 6 (1973).

16. R.K. SARMA, N.H. CHAN, and D.M. SMYTH, "Solubility of TiO_2 in $BaTiO_3$", J. Am. Ceram. Soc., Vol.64, [8] 448 - 51 (1981).

17. T. NEGAS, R.S. ROTH, H.S. PARKER, and D. MINOR, "Subsolidus Phase Relations in the BaO-TiO_2 System", J. Solid State Chem., Vol.9, [3] 297 - 307 (1974).

18. P. BAXTER, N.J. HELLICAR, and B. LEWIS, "Effect of Additives of Limited Solid Solution on Ferroelectric Properties of Barium Titanate Ceramics", J. Am. Cer. Soc. Vol.42, [10] 463 (1959).

19. J.M. HONIG and C.N. RAO, Preparation and Characterization of Materials, Academic Press, 217 - 247 (1981).

20. L.WU, T.S. WU, and C.C. WEI, "Dielectric Properties of Barium Titanate Modified with Certain Substitutes", unpublished.

21. D.E. WITTMER and R.C. BUCHANAN, " Low-Temperature Densification of Lead Zirconate - Titanate with Vanadium Pentaoxide Additives", J. Am. Cer. Soc., **64** [8] 485 - 90 (1981).

22. H.U. ANDERSON, "Sintering of LiF fluxed $SrTiO_3$", Sintering and Heterogeneous Catalysis; Materials Science Research, Plenium Press, Vol.16, 281 - 92 (1984).

23. D.E. RASE and R. ROY, "Phase Equilbria on the System Bao-TiO_2", J. Am. Cer. Soc., Vol.38, 102 - 113 (1955).

24. L.K. TEMLETON and J.A. PASK, "Formation of $BaTiO_3$ from $BaCO_3$ and TiO_2 in Air and in CO_2", J. Am. Cer. Soc., **42** 212 - 216 (1959).

25. P.K. GALLAGHER and F. SCHREY, "Thermal Decomposition of Some Substituted Barium Titanyl Oxalates and its Effect on the Semiconducting Properties of the Doped Materials", J. Am. Cer. Soc., Vol. 46, 567 - 573 (1963).

26. B.J. MULDER, "Preparation of Barium Titanate and Other Ceramic Powders by Coprecipitation of Citrates in an Alcohol", Am. Cer. Soc. Bull., **49** 990 - 993 (1970).

27. T.J. CARBONE and J.S. REED, "Microstructure Development in Barium Titanate : Effects of Physical and Chemical inhomogeneities", Am. Cer. Soc. Bull., **58** 512 - 515 (1979).

28. D.L. JOHNSON, "Solid-State Sintering", Encyclopedia of Materials Science and Engineering, The MIT Press, **6** 4520 (1986).

29. W.D. KINGERY, "Densification During Sintering in the Presence of Liquid Phase", J. Applied Physics, **30** [3] 301 - 6 (1959).

30. R.L. COBLE, "Sintering Crystalline Solids; I. Intermediate and Final Stage Diffusion Models", J. Appl. Phys., **32** [5] 787 - 92 (1961).

31. D.M. TROTTER, "Capacitors", Scientific American, 86 - 90 July (1988).

32. A.R. VON HIPPEL, Dielectric Materials and Application, John Wiley and Sons, Inc. (1954).

33. Ceramic Test, J. Am. Cera. Bull., 370pp (1958).

34. M.I. MENDELSON, 'Average Grain Size in Polycrysatlline Ceramics", J. Am. Ceram. Soc., **52** [8] 443 - 6 (1969).

35. B.D. CULLITY, Elements of X-ray Diffraction, Addison-Wesley Inc., 2nd Edition, Chpts.2,3 (1978).